# CFD MODELLING OF FLOW AT THE EPIGLOTTIS

Matthew Berry

Bachelor of Engineering
Mechanical Engineering


Department of Engineering
Macquarie University

November 6, 2017

Supervisor: Dr. Shaokoon Cheng

**ACKNOWLEDGMENTS**

I would like to acknowledge my academic supervisor Dr Shaokoon Cheng for guiding me throughout the duration of the project and allowing me to undertake it at my own pace. I would also like to acknowledge Joel Raco and James Li for all the time they have given up in order to help me progress through the project and assist me in the learning of the required software programs for the project.

**STATEMENT OF CANDIDATE**

I, Matthew Berry, declare that this report, submitted as part of the requirement for the award of Bachelor of Engineering in the Department of Engineering, Macquarie University, is entirely my own work unless otherwise referenced or acknowledged. This document has not been submitted for qualification or assessment an any academic institution.

Student's Name: Matthew Berry

Student's Signature: MATTHEW BERRY

Date: 6/11/17

## ABSTRACT

The upper airway is an important component of the human body; particularly the epiglottis and surrounding region. Studies have shown that in terms of retaining of drug particles, the epiglottis is the most prominent region involved. However, a significant amount of research has not been completed in order to investigate and define a potential relationship between epiglottis geometry and airflow through the region. This project will involve the creation of upper airway models and airflow simulations to determine whether a relationship exists, potentially laying a platform for new methods to be developed with respect to drug particle retention within the region.

# Contents

# List of Figures

# List of Tables

# Chapter 1

# Introduction

The upper airway is a complex structure within the human body. The epiglottis is a key feature of the upper airway system, and plays a crucial role by ensuring that air and food will reach its intended destination within the body. Another role which the epiglottis plays is the retention of drug particles which have been inhaled. Minimal research has been done concerning this area, and thus, there are uncertainties about how drug particles are retained within the upper airway system. Therefore, the effectiveness of some medicinal drugs is compromised due to a lack of understanding of the function of the epiglottis. The upper airway system is unique and its geometry can vary from person to person, and thus, it is important to research this area in order to allow effective treatment to be administered to all patients, despite the differences in their upper airway geometry.

## 1.1 Project Outline

The project itself will involve a number of activities which will be undertaken in order to complete the project and answer the research question. First, a model of the upper airway will be constructed using a software program called "3D Slicer". An understanding of how to use the software will have to be developed first in order to create the model. Once the model has been completed, the file will have to be converted in order to be used on Computation Fluid Dynamics (CFD) software. Some understanding will also be developed in order to use the software, before simulating airflow through the upper airway. Results will be produced from

this simulation and a discussion will result in order to determine a possible relationship between upper airway geometry and airflow, and subsequent conclusions can be drawn.

This project is entirely software based as it is the most feasible method of investigating the designated area. If this project were to be undertaken in the real world, human subjects would be involved, and a number of sensors would have to be fitted in various areas throughout the subject's upper airway system in order to measure parameters such as; velocity, pressure and temperature. If the project were to be undertaken in this way, it would be unfeasible due to limited access to the upper airway, and also unethical due to the possible consequences of failure. Therefore, software analysis is the most feasible method to undertake this particular project.

# Chapter 2

# Background

## 2.1 Upper Airway Anatomy

There are a number of different components in which the upper airway can be broken down into. The pharynx is one of the most prominent features of the upper airway. It covers the middle portion of the overall system – with the entrances considered being the mouth and nose and exits being both the larynx and oesophagus [1]. For a typical adult human, the pharynx is approximately 12-15 centimetres in size [1]. Subsequently, the pharynx can also be broken down into a number of components – the nasopharynx, the velopharynx, the oropharynx, and the hypopharynx [1].

One entrance to the upper airway system is the nasal cavity, or the nose. The cavity begins with two separate channels (the nostrils), separated by the septum, and the nasal vestibule region [2]. Located behind this region is the narrowest part of the nasal cavity – the nasal valve region [2]. From here follows the main airway channels, which are much larger than the previous regions [2]. These channels are bordered by the superior, middle, and inferior turbinates – bone-like folds which separate and divide the region [2]. Beneath these turbinates are smaller passages known as "meatuses", and are named according to the surrounding turbinate [2]. Located at the top of this region is the olfactory region which allows access between the nasal cavity and the nervous system [2]. As the nasal cavity reaches the nasopharynx, the two nasal airway channels meet and become one channel [2].

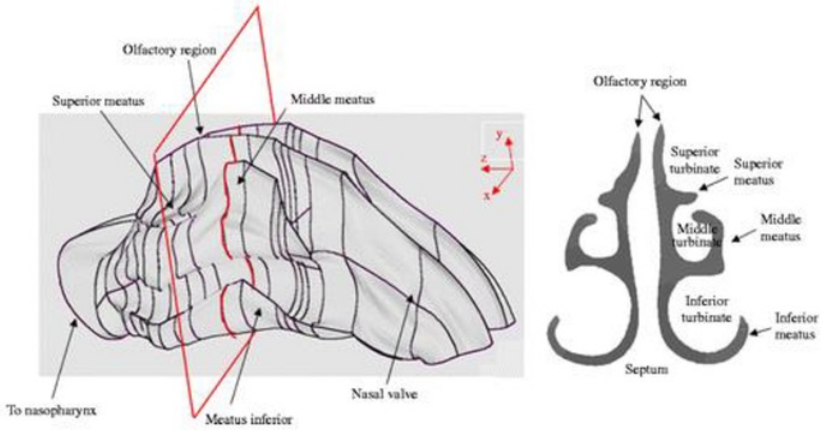


**Figure 2.1:** Features of the nasal cavity

The other entrance to the upper airway system is the oral cavity, also simply known as the mouth. The walls of the cavity act as the border of the cavity itself to separate it from other components of the upper airway system. The roof of the oral cavity consists of a hard palate towards the front and a soft palate towards the rear [1]. The floor of the mouth is the lingual mucosa and the walls are the buccal mucosa [1]. The mucosa creates the desired flexibility of the particular areas to allow for everyday tasks, such as chewing, speaking or swallowing, to be performed [3]. When describing the location of a particular component of the pharynx, its location is often described with respect to the oral cavity, using it as a point of reference.

The pharynx is a major component of the upper airway system, and can subsequently be broken down into subcomponents, with the first being the nasopharynx. It is located above the oral cavity, and all the other components of the pharynx, and is located within the nasal cavity [1]. The next component is the velopharynx, which is located directly below the nasopharynx, and behind the oral cavity [1]. More specifically, it is located directly behind the soft palate region of the oral cavity [1]. The velopharynx can be considered as the junction where the oral and nasal cavities intersect each other. The oropharynx is the next component, and it houses the area between the soft palate and the epiglottis [1]. It has a

typically larger cross-sectional area than that of the velopharynx [1]. The final component of the pharynx is the hypopharynx, which covers the area between the epiglottis and the glottis [1]. It starts at the base of the tongue and travels alongside the oesophagus.

The larynx is a continuation of the upper airway system, and leads toward the lower airway system, trachea (located towards the front), and eventually into the lungs [1]. Another exit of the pharynx is the oesophagus (located towards the back) which is separate to the upper airway system as it leads towards the stomach [1]. The role of the epiglottis therefore, is to open to allow air to travel through the trachea, and close to allow food and liquid to travel through the oesophagus.

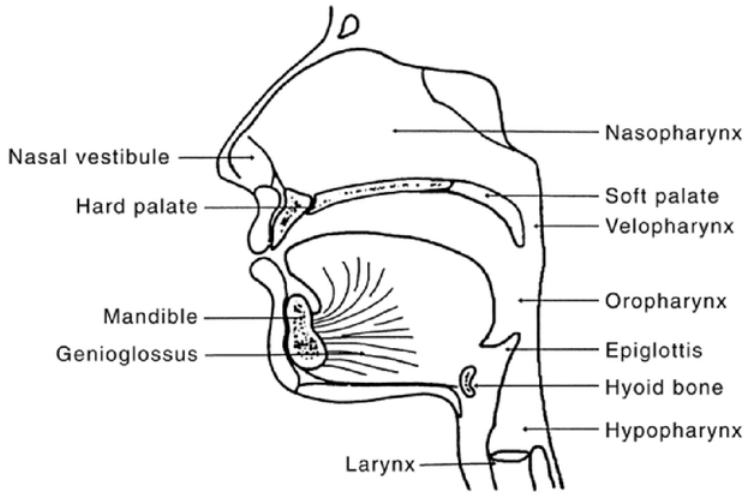


**Figure 2.2:** A detailed diagram with the location of the upper airway system components [4]

## 2.2 Upper Airway Physiology

The upper airway system works effectively with the surrounding bones and muscles to allow air entering the nose or mouth to travel through to the trachea, and subsequently into the lungs. Air enters the nose and into the nasal vestibule, and then into the nasal valve region where the air reaches its largest velocity [2]. It then expands into the main airways region and through the meatuses [2]. From here, it continues to flow through the rest of the nasal cavity and subsequently through to the lungs. This process usually occurs within 4-5 seconds, and the flow rates can vary depending on how light or heavy the breathing is [2]. The nasal vestibule will also collapse to cope with larger flow rates which could be a result of sniffing or some other form of sharp breathing [2]. The palatal muscles are responsible for determining whether airflow will enter from the mouth or the nose [4]. Air flow generally occurs through the nose when the body is at rest as it is more efficient, however, during exercise or other activities which induce relatively heavy breathing, the air will flow through the mouth due to the higher airflow resistance which occurs in the nasal valve [4][5]. Breathing through the mouth though creates a number of disadvantages to the functions of the upper airway system, such as a decreased efficiency of heating, humidification, and filtering of the air passing through [4][5]. The internal walls also need assistance from the surrounding muscles in order to create stability due to the forces created by the air which passes through [4].

The genioglossus muscle is an important function. It moves the tongue in such a way that more space is created behind the tongue to help aid the inspiration (breathing in) process [4]. However, as an effect of the genioglossus muscle, resistance can subsequently occur at the hypopharynx, and also as a result of the mandible bone [4].

The major objective of the upper airway system during expiration (breathing out) is to slow down the airflow travelling through, as this allows for a longer time for the gas to be exchanged at the alveoli within the lungs [4]. To help achieve this, the surrounding muscles can narrow the area of the pharynx in order to create more resistance, causing a braking effect of the airflow as it leaves the system [4]. The nasal valve can also work in a similar way to act as a brake [4].

## 2.3 Using Inhaler Device as Treatment

There is a long history associated with using inhalers as a form of treatment, with records of using such a device being traced back some four thousand years ago [6]. Britain has records of using such a device to treat asthma dating back as far as the 1800s [6]. Using inhalers has been used primarily as a treatment for asthma, but can also be used for a wide range of respiratory problems. Inhaler devices were introduced to provide a much more direct and effective method of delivering treatment to the lungs [6]. One advantage over existing methods, such as tablets and other oral methods, is that smaller doses would be required, resulting in a lower risk of overdose and greater cost-effectiveness [6]. Another major advantage over existing methods is that the treatment is much more direct, meaning that the drug is delivered directly to the lungs without affecting other irrelevant parts of the body and reducing the possibility of causing side-effects [6].

## 2.4 Problems with Drug Particle Delivery

While using inhalers as treatment is indeed an effective method of delivering medicinal drugs directly to the lungs, and much research is constantly being done in order to improve the effectiveness, there are still some factors which are yet to be addressed which can hamper the overall effectiveness of delivering these drugs. One major issue is the lack of personalisation for each individual patient, with differing results being produced from person to person. Table 1 highlights the factors which can determine the overall effectiveness of an inhaler device, and a number of which relate to the device itself. However, there are some factors present which relate entirely to the individual, thus leading to a difference in effectiveness from one individual to another.

The delivery of the drug particles through the system is determined by two major factors. One of these factors is the turbulence created by the device itself, but the other is the inspiration produced by the patient themselves, highlighting the importance of personalisation among

these particular devices. The generated force would vary from person to person, and could even vary from one dose to another, even when applied to the same individual. There must be a balance struck between the two main forces in order for the most effective results to be produced. For example, breathing in too fast or too slow would produce an abnormal force and subsequently affect the delivery of the drug particles and produce a less than satisfactory result [7]. Another issue to consider is that air flow inhalation is affected on the breathing capacity of the patient [7]. However, given that the patient requires an inhaler device in the first place would mean that their breathing capacity is already potentially hampered. This concern would also relate to the issue of personalisation.

Another factor which should be considered when designing an inhaler device (as mentioned in Table 1) is respiratory tree geometry. The factors mentioned above, such as breathing rates and other forces, can ultimately be controlled by the patient. Respiratory tree geometry and configuration however, cannot be controlled by the patient. The structure and various measurements (diameters, lengths, angles etc.) affect parameters such as pressure, velocity and temperature within the upper airway system, and therefore affect the overall effectiveness of the delivery of the drug particles to the lungs, thus highlighting the importance of personalisation when concerning inhaler devices.

Table 2.1: The parameters which must be considered when designing an inhaler device [8]

| **Properties** | **Parameters** |
|---|---|
| Aerosol properties | Mass median aerodynamic diameter |
| | Geometric standard deviation |
| | Fine particle fraction |
| | Air/particle velocity |
| Particle properties | Volume diameter |
| | Bulk density |
| | Tap density |
| | Shape |
| | Charge |
| Physicochemical properties | Solubility |
| | Hygroscopicity |
| Lung properties | Geometry of respiratory tree (airway structure and diameter of airways) |
| | Influence of disease state on airway structure |
| | Breathing pattern – mouth or nasal breathing |

## 2.5 Experimental Work/Computational Modelling

In order to further investigate the issues of upper airway geometry affecting the airflow, studies are currently being undertaken [9][10]. Thanks to programs such as Computational Fluid Dynamics (CFD), virtual models can be created and simulations can be run in order to further analyse features such as airflow. Given that the upper airway geometry is indeed quite complex, programs such as CFD have allowed the analysis to take place with a lot more ease and convenience when compared to undertaking a physical experiment [9]. These programs are available at little or no financial cost and can provide highly accurate and detailed results [9]. Also, as mentioned previously, it is a much more feasible option than preforming a physical experiment given the sheer difficulty and also ethical considerations of placing sensors or some similar device inside a human subject. These modelling techniques have so far proven that the upper airway geometry does indeed have an effect on the airflow through the upper airway system, but work is continually being undertaken to investigate further [10].

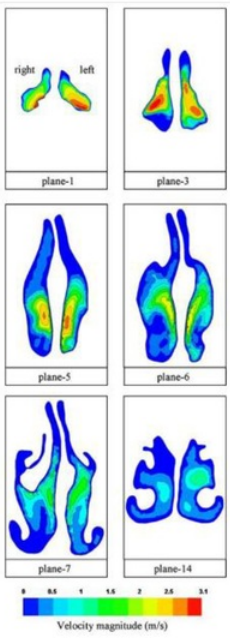


**Figure 2.3:** Velocity contours of the nasal cavity produced using CFD [9]

# Chapter 3

# Experimental Method

This section of the report will document the process which was followed in order to complete the project. Activities such as; creating the model, converting the file, and CFD simulations will be described in order to provide an in-depth review of the process required to complete the activities of the project.

## 3.1 3D Slicer

This sub-section will document the process which was followed in order to create the model of the upper airway which will be required to perform the later simulations. This process uses purely the 3D Slicer software.

### 3.1.1 Basic Functions of 3D Slicer

Before creating the model, a basic understanding of how to use the software had to be developed. The program can be downloaded at no cost from download.slicer.org, and the particular version used was version 4.7.0-2017-08-18.

Once the program has been downloaded, the figure 3.1 shall appear when the program is opened.

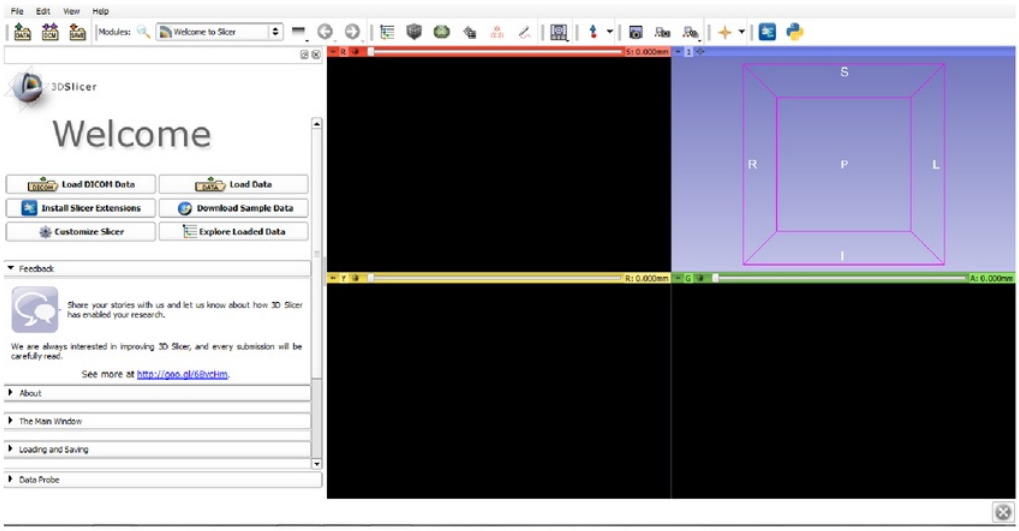


**Figure 3.1:** Home screen when Slicer first opens

Once Slicer opens, click "Load Data" on the left hand side of the screen, then "Choose File(s) to Add". Find the appropriate .nrrd file and click "OK".


**Figure 3.2:** The highlighted "Load Data" icon

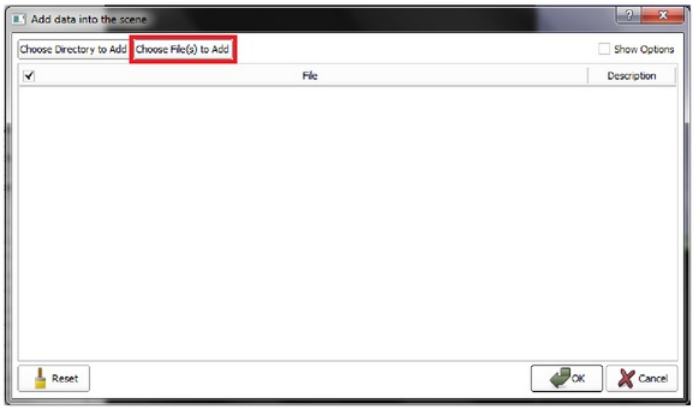


**Figure 3.3:** The "Choose File(s) to Add" icon to allow user to find the desired file

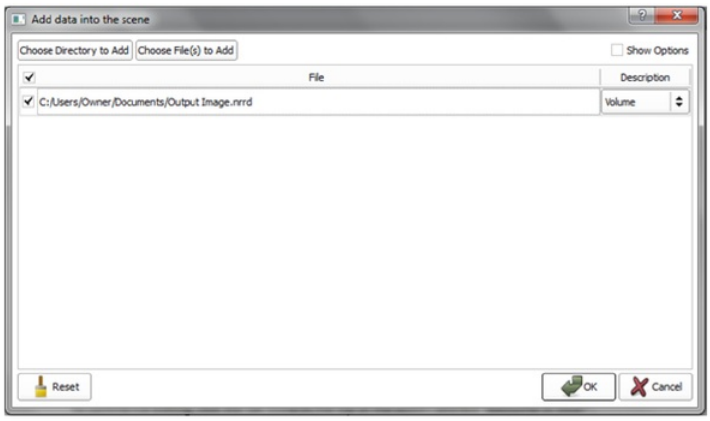


**Figure 3.4:** Display screen once the desired file has been chosen

Now, the images should appear on with the three views as shown in figure 3.5 below.

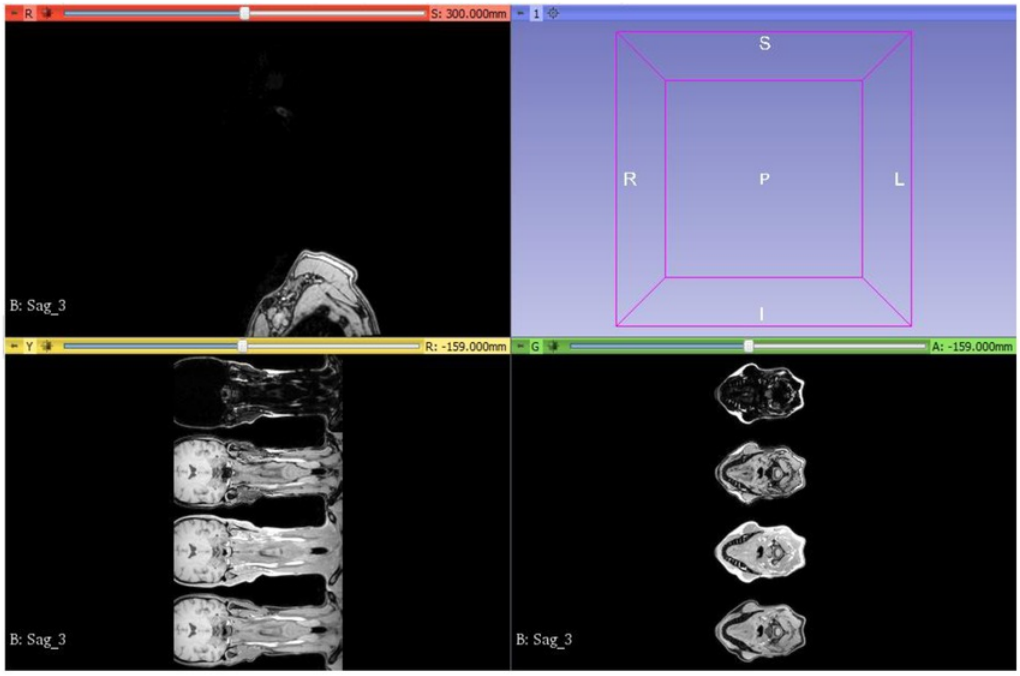


**Figure 3.5:** Display screen once the file has been completely opened

The number located at the top-right of each view (i.e. S: 300.000mm, R: -159.000mm and A: -159.000mm) indicate what "slice" is currently being displayed. Moving the scroll wheel on the mouse allows the user to scroll through the slices which will appear on the respective screen. Clicking and holding the left mouse button while moving the mouse will alter the brightness of the image, and clicking and holding the right mouse button while moving the mouse will zoom in and out. The aim of using Slicer is to predominantly use one particular view (Axial, Sagittal or Coronal) and highlight the desired area, ensuring the highlighted area covers all the slices of the image.

### 3.1.2 Resizing the Image

Because the image is quite large, and much of it is unnecessary, it is useful to resize the image in order to produce an image which will focus more on the upper airway specifically. Also, this method can increase the number of pixels allowing for a more accurate model to be created.

First, click the tab at the top of the screen labelled “Welcome to Slicer”, then select “All Modules”, and then “Crop Volume”. This is to select purely the upper airway system and remove unnecessary parts of the image.

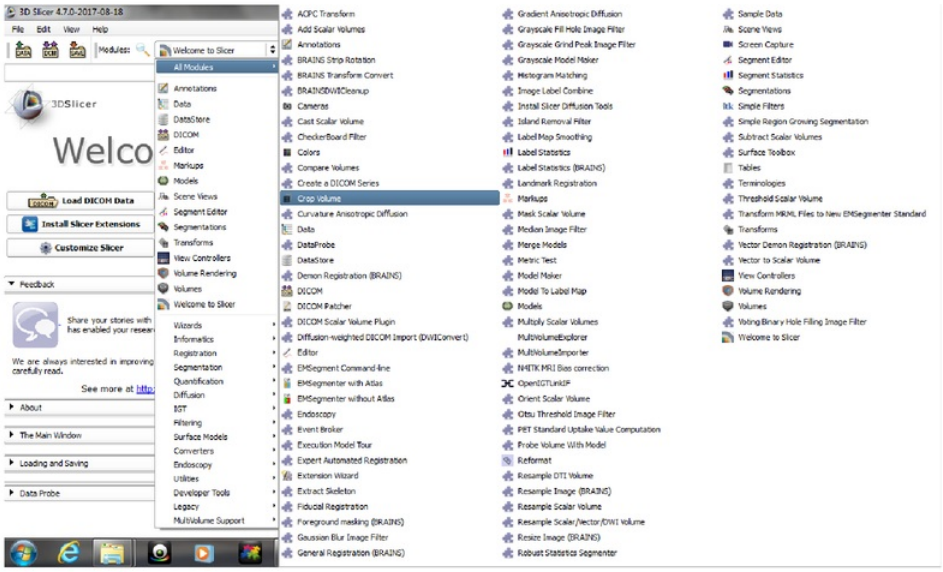


**Figure 3.6:** The display screen showing the location of “Crop Volume”

Set the “Input ROI” function to “Create new Annotation ROI”, and ensure the parameters are set accordingly. The box on the image views is also altered to house only the upper airway system. Once the settings are as shown as below, select “Apply” at the bottom of screen.

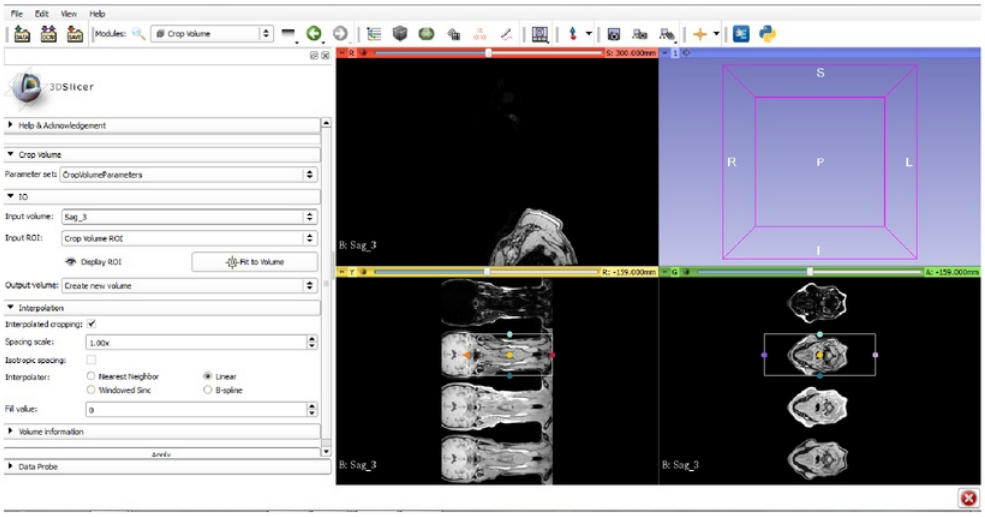


**Figure 3.7:** Display screen showing the desired settings

Once this has been completed, again select the tab at the top of screen, and find "Resize Image (BRAINS)" as shown. This tool will allow for the increase in the number of pixels, so that a greater accuracy can be achieved when drawing/highlighting the desired parts of the image.

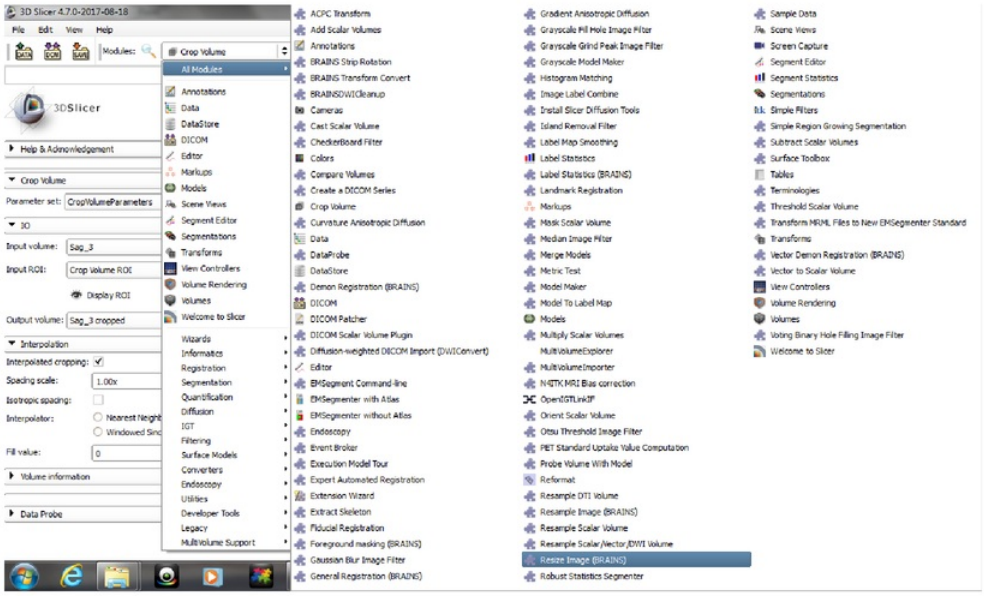


**Figure 3.8:** Display screen showing the location of "Resize Image (BRAINS)"

The "Image to Warp" parameter is set to the original file name with the word "cropped" added to the end of it, i.e. in this case, the original file name was "Sag_3", so the chosen parameter was "Sag_3 cropped". Also, the option for "Output Image" was set to "Create new Volume". The "Scale Factor" is also set to 0.5 in order to multiply the number of pixels by two. "Apply" is then selected.

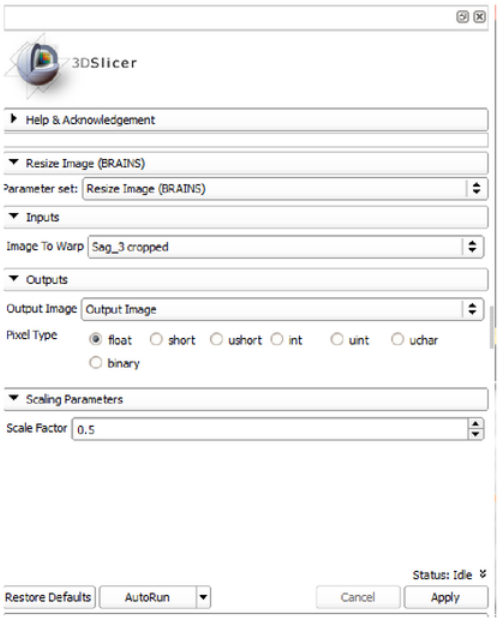


**Figure 3.9:** Display of the appropriate settings which were used

### 3.1.3 Creating the Model

Once the resizing of the image has been completed, the file name is now "Output Image.nrrd". Slicer must be closed and re-opened, and the new file is loaded into the program as before.

To commence editing, click the tab towards the top-left of the screen labelled "Welcome to Slicer". Choose "Segment Editor" from the list of options which appear from the tab.

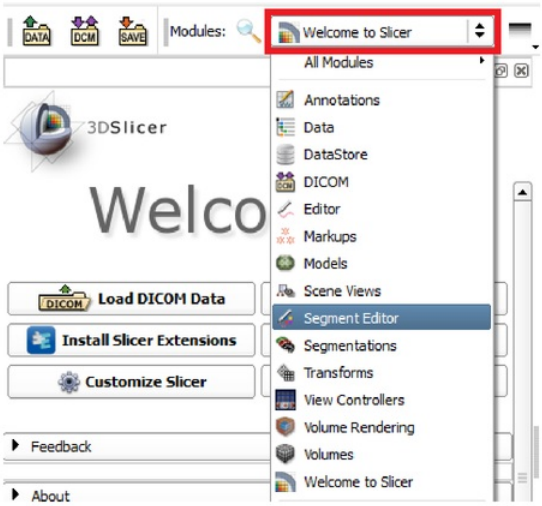


**Figure 3.10:** Tab where "Segment Editor" is located

Now that Segment Editor is open, editing can now take place. First, ensure the "Segmentation" option is set to "Segmentation", and ensure that "Master Volume" option is set to the same file name of that of the .nrrd file which was previously selected. This allows editing to take place on the desired image. Then, click "Add segment".

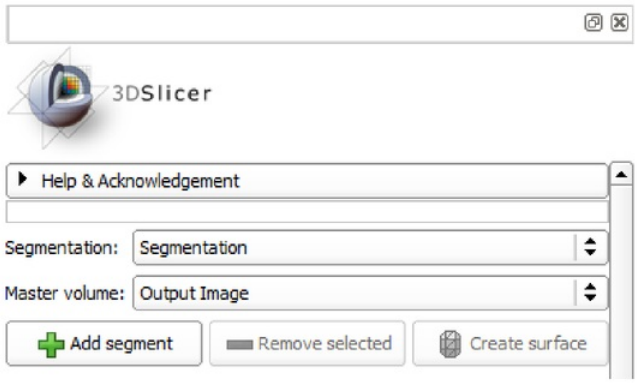


**Figure 3.11:** Display showing the settings required to commence editing

"Segment_1" should now appear, and a range of editing effects is now available.

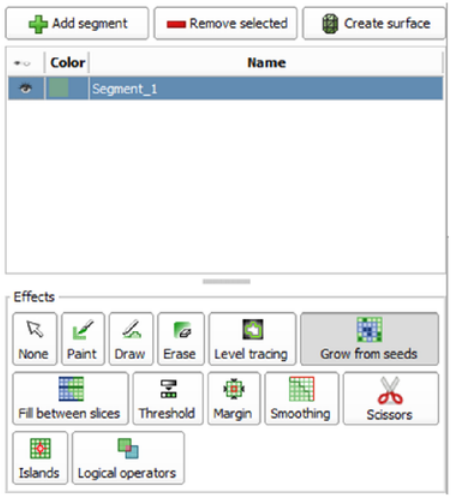


**Figure 3.12:** Display screen of the various editing effects

The "Paint" function can be used in order to roughly sketch certain areas. This is useful if the desired area is quite large. The "Draw" function allows the user to trace the desired shapes using the mouse. Click and hold the left mouse button while tracing the shape, then click the right mouse button when complete. The shape is now highlighted. This is useful to highlight much finer areas. The "Erase" function works the same way as the "Paint" function, except it removes certain areas rather than highlighting them. The "Level Tracing" function is also used to automatically highlight large areas of the same colour. Once selected, hover the cursor over the image, and a yellow outline will appear around corresponding areas of the image. Once the desired area is achieved, click the left mouse button to highlight the area.

To create the model, the sagittal view was predominantly used. The first slice chosen was where the nasal cavity first begins. The area was highlighted using the techniques mentioned above. Then, scroll through 5mm (approximately 20 slices), and highlight the desired area on that particular slice. This process was repeated until reaching the pharynx (end of the nasal

cavity). Then, the function "Fill between slices" is selected, and then "Initialize". This process will highlight all the slices in between the slices which were drawn on. This process will create a model of the nasal cavity.

To model the pharynx and larynx, a different method will be used. First, select "Add segment", and another segment shall appear on the list underneath the first segment. The option "Threshold" is selected from the range of effects, and the eye icon next to the segment name is closed.

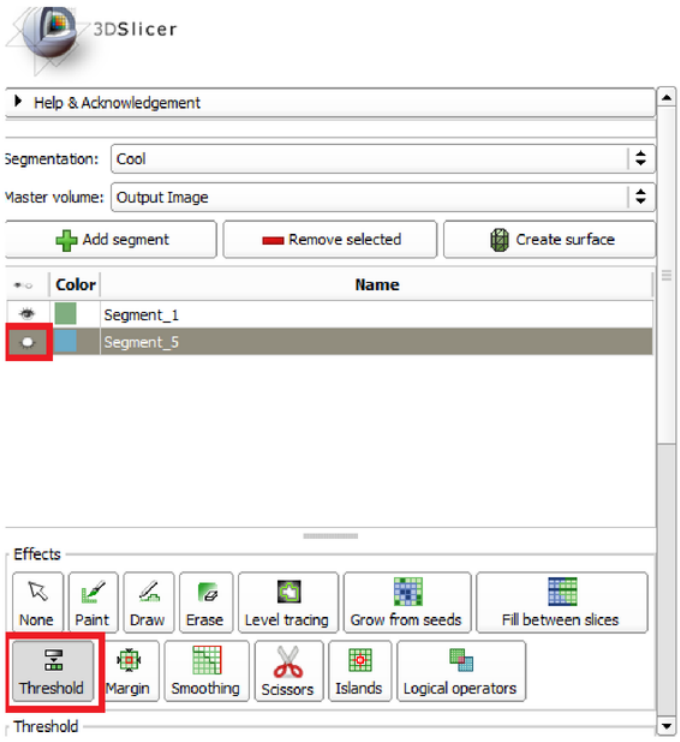


**Figure 3.13:** Display showing the "Threshold" option and the closed eye icon

The threshold range must now be set in order to highlight desired areas. The lower limit is set to zero, whereas the upper limit can be set to a variety of different values

in order to achieve the most accurate highlighted area. This method is used in order to achieve an accurate model of the epiglottis area in particular. This area was analysed in particular when determining the upper limit of the threshold. Once the limits are chosen, the "Editable area" option is set to "Outside all visible segments", and "Overwrite other segments" is set to "All segments", and then "Apply" is chosen.

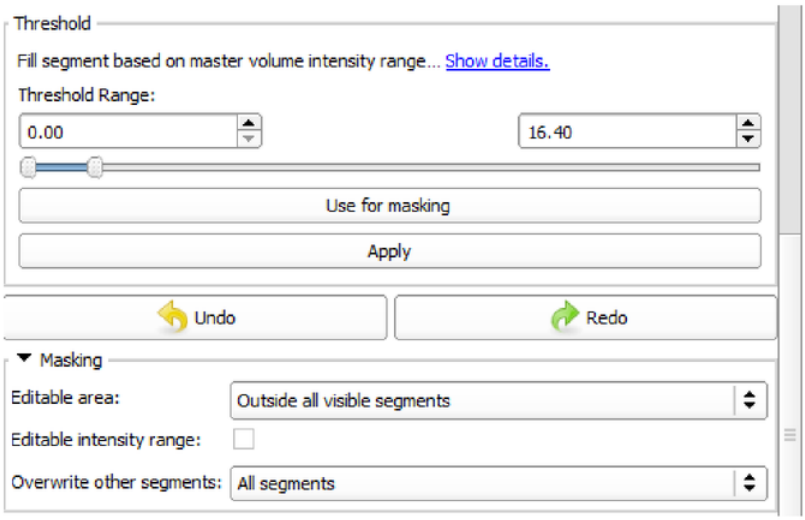


**Figure 3.14:** Display showing the "Threshold" option settings

The eye icon next to the second segment is then set to open, and is now visible on all the slices. There is much excess material which must be removed. This is done using the "Scissors" effect. While the "Erase" effect is only applicable to the particular slice, the "Scissors" effect applies to all slices, so care must be taken in order to avoid removing material which is not unnecessary. The scissors effect can be used on any of the three views, or the "Create surface" option can be selected, where a three dimensional model will be produced, and material can be removed from that.

Once the excess material is removed, there are two segments – one for the nasal cavity and another for the larynx and pharynx. To merge both into one segment, the first segment is

selected, the "Logical operators" option is chosen, "Operation" is set to "Add", the second segment is highlighted under "Add segment", and then "Apply". The two segments are now the same colour, and the model is complete.

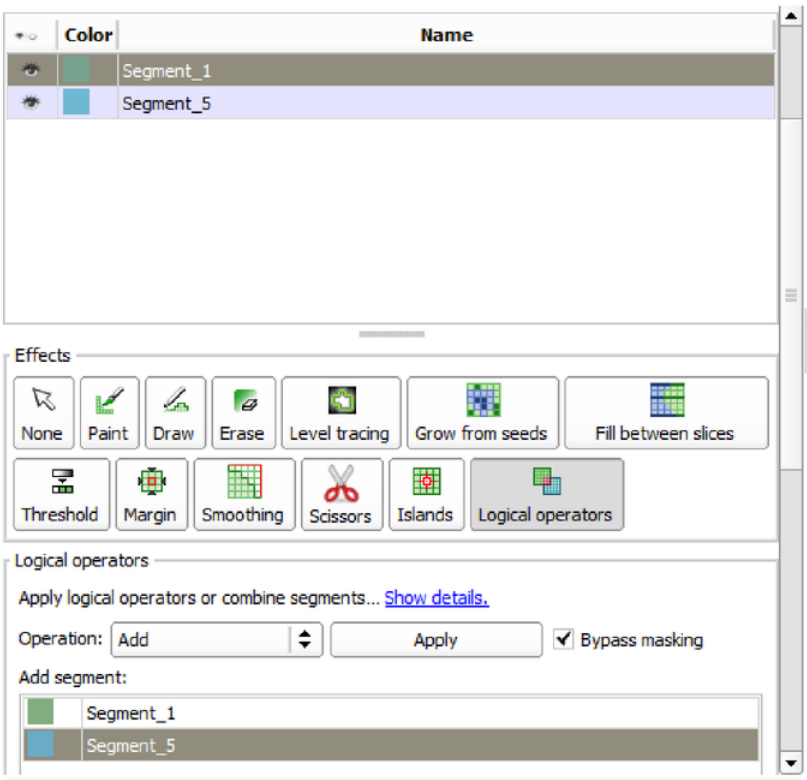


**Figure 3.15:** The "Logical Operators" option and settings

### 3.1.4 Saving the Model

Once the model is complete, all the necessary files must be saved. The "Save" icon located at the top-right of screen is selected. Then, a list of files appear, where the "MRML Scene" file and the "Segmentation" file must both be saved, but the "NRRD" file is not required to be saved. The appropriate boxes are ticked accordingly, and then saved.

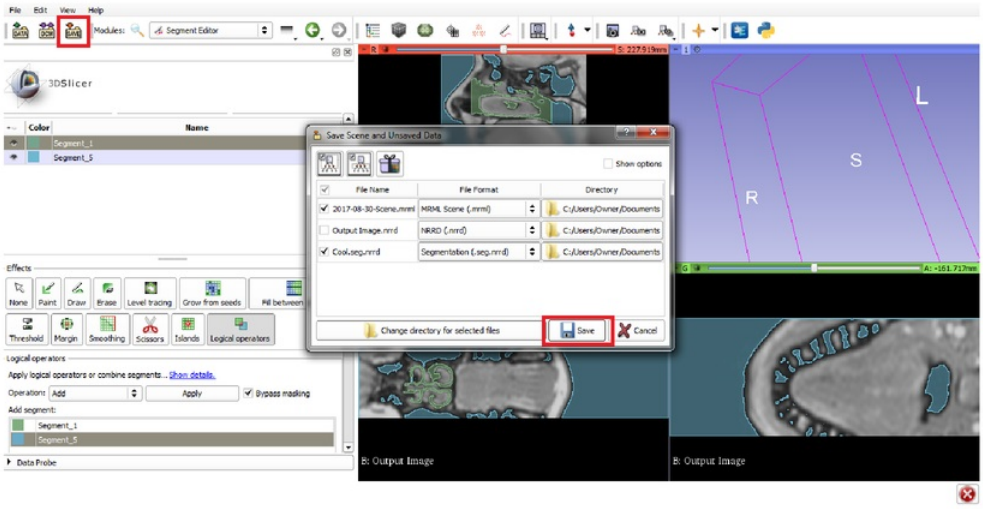


**Figure 3.16:** Display screen showing the save options

## 3.2 Converting the File

This subsection will detail how the file was converted in order to be opened in CFD.

Before converting the model, Slicer was still required in order to correctly export the file to be opened using another program. The model had to be exported in the correct format by first selecting the “Segmentations” option from the drop-down tab at the top left of screen.

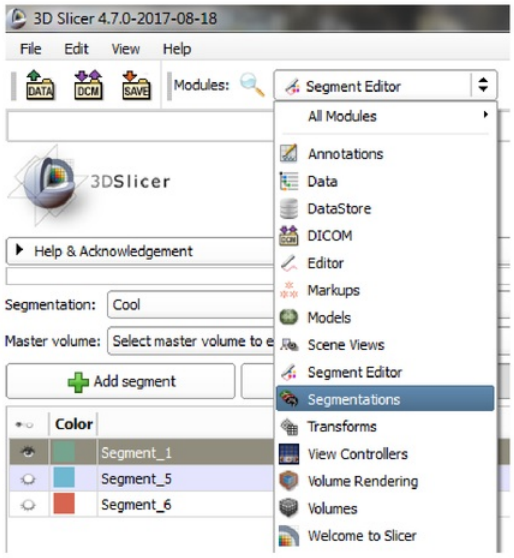


**Figure 3.17:** Location of the "Segmentations" option

The "Active segmentation" option was ensured to be the same name as the original model file, and the eye icon next to all other segments (if applicable) are still set to "closed".

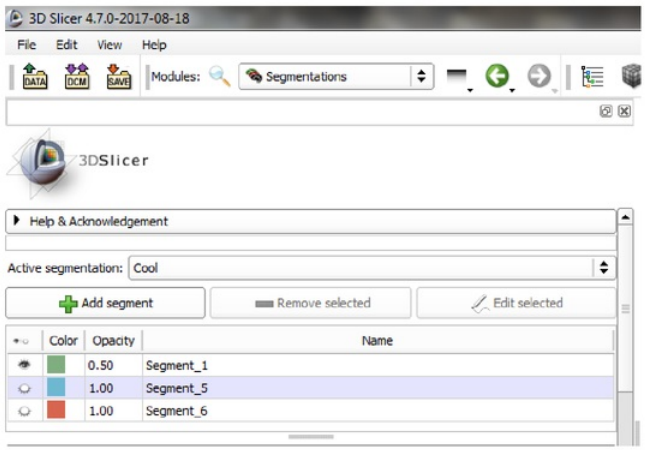


**Figure 3.18:** "Active segmentation" and the closed eye icons next to unnecessary segments

The next setting required was the "Export/import models and labelmaps", where "Operation" is set to "Export", "Output type" is set to "Models", and "Output node" is set to "Export to new model hierarchy". Also, under the "Advanced" settings, "Exported segments" is set to "Visible". Then, the "Export" function is selected.

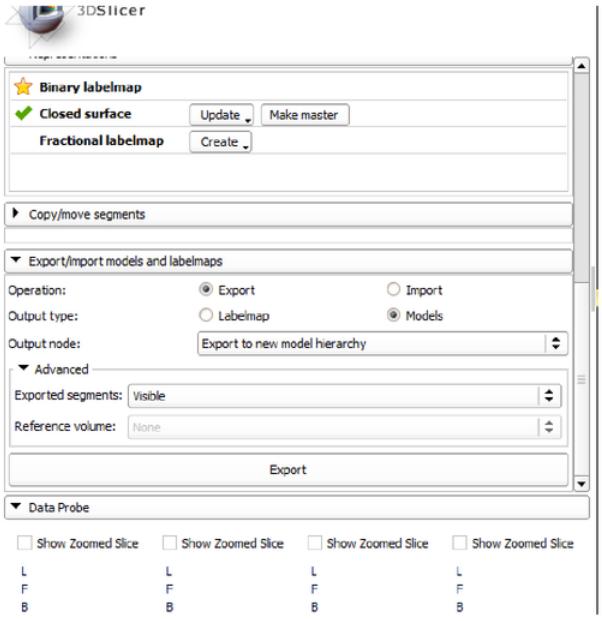


**Figure 3.19:** The appropriate settings required to export the model

Once the settings are chosen, the "Save" icon was selected at the top left of screen. The "Segmentation" file was renamed in this case simply to avoid any confusion, but was not necessarily required to be renamed, and also the "Segment_1" file was changed from a ".vtk" file to a ".stl" file.

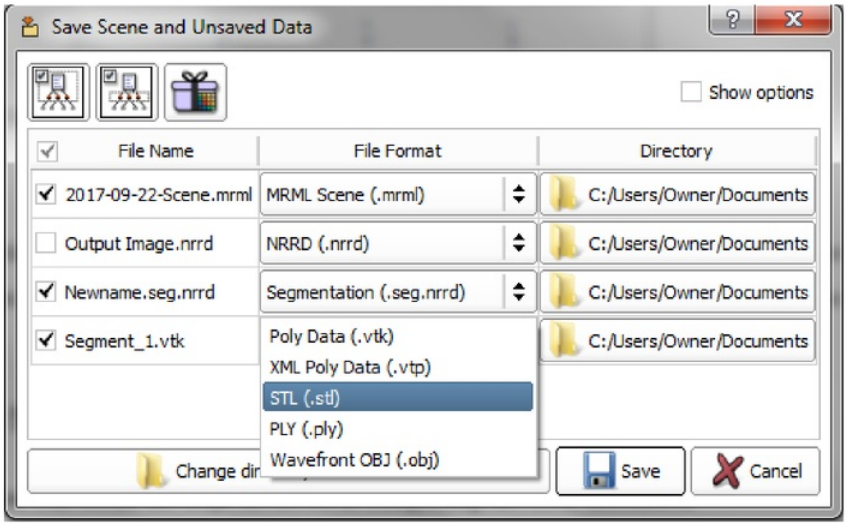


**Figure 3.20:** Appropriate settings to save the file

Now that the file has been exported as an .stl file, 3D Slicer is no longer required for the project. A program named "Rhinoceros" will now be used in order to modify and convert the file to allow for use in ANSYS (ANSYS version 18.1 will be used for simulation).

First, the program was opened as normal, and the Slicer file was opened by selecting "Open" from the "File" tab at the top left of screen. The file should now open and four different views of the model should now be visible.

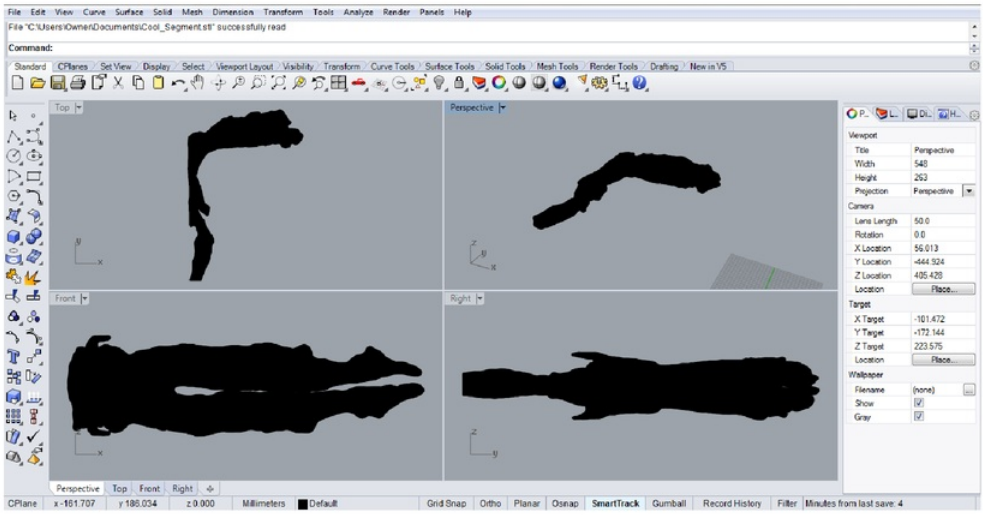


**Figure 3.21:** The model opened in Rhinoceros

Using the cursor, a box is drawn around any of the four views to highlight the entire model. The four images of the model now appear yellow in colour to indicate that the entire model has been selected. The option “Shade” is selected from the tab above the model. This option is applied to the model in order to give the model a more solid appearance, rather than a hollow appearance.

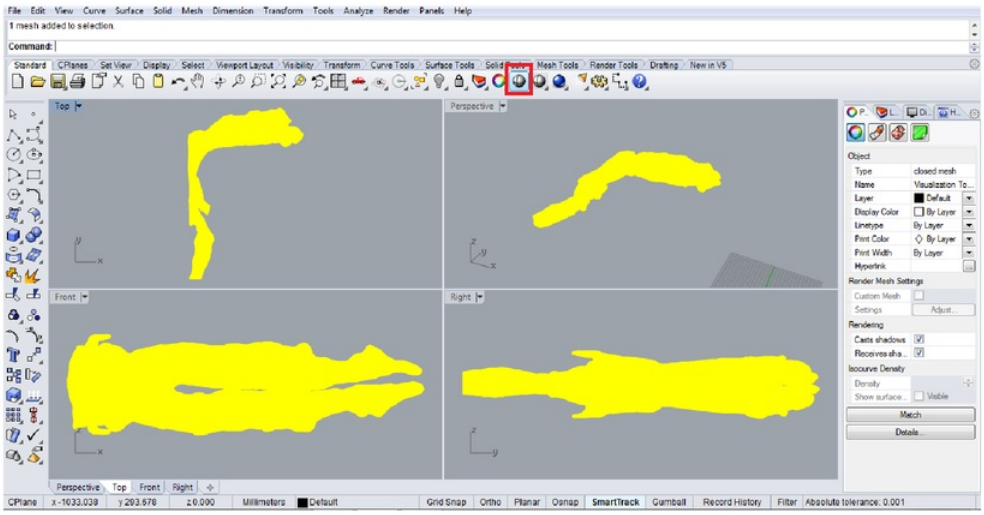


**Figure 3.22:** The yellow, highlighted model and the location of the "Shade" function

Once the "Shade" function had been used, the model is now ready to be exported. The model is simply saved under "Save As…" where it is saved as a "Rhino 5 3D Models" file (.3dm file). This is the file which will be used for the CFD analysis in the next step of the project.

## 3.3 CFD Simulation

### 3.3.1 Mesh Convergence

Before the analysis can commence, the mesh convergence must be ensured to determine whether the results are dependent on the mesh or not. A CFX project was first commenced using the newly created model file from Rhinoceros in the previous step of the project. The mesh was setup in a normal manner with boundary conditions set, such as the two nostrils as the inlets and the throat area as the outlet. The key feature of the mesh convergence process is the option within meshing "Max Face Size". This option allows for the increase/decrease of

the individual shapes which make up the total mesh, therefore altering the density of the total mesh. Varying values were chosen to steadily increase the mesh density as this process was completed. Once the value was chosen, the number of nodes and elements was recorded individually, and the meshing component was now concluded.

Basic settings were used for the setup of the simulation, with a constant velocity being chosen and used throughout. Once the setup had completed, the simulation was run to simulate air flow through the model at a steady-state condition.

For the results, a reference line was created towards the bottom of the model around the throat area, running from the front to the back (in the x direction). The results involved breaking down this line into 25 smaller points at which the air velocity in the y direction was measured. The results produced indicated the velocity at each of the 25 points along the line, and also a curve highlighting the differences in velocity along the line of reference. The velocity at the middle point and also the maximum velocity were both recorded, and an average was also taken for all 25 points on the line.

This process was repeated using decreasing maximum face sizes to represent an increase in mesh density. All the results from each mesh density were compiled into a table. Graphs were created to plot either the middle point velocity or the maximum velocity versus the maximum face size. Also, all the points along the line of each corresponding maximum face size were compiled together to create another graph to also demonstrate mesh convergence. Once it was determined that there was evidence of mesh convergence, the simulations can continue to be run.

### 3.3.2 Steady-State Conditions

The process taken for the steady-state conditions followed a similar process to that of the mesh convergence. The model file was imported and the mesh was modified in a similar way. The max face size was altered to 0.0021, and the inlet was set to be the two nostrils, and the outlet being at the bottom of the throat. For the setup, the inlet velocity was chosen to be

3m/s split between both nostrils, with the k-epsilon method being used and also a no-slip wall condition. The simulation was run with these basic settings applied and results were produced.

### 3.3.3 Transient Flow Conditions

The process followed for these conditions were not too dissimilar to the steady state conditions. The simulation itself was linked to the steady state simulation with some minor modifications being made to the simulation settings. The inlets and outlets were set as previously done, but the key difference was to use inflation, with 5 layers as the setting. Another key difference being that in the setup phase of the simulation, both the inlets and outlets were set as an "opening" rather than simply an inlet or outlet. Also, instead of a constant velocity being used, a sine wave was used to represent the inlet velocity. The function had to first be created within the setup before being applied to the model simulations. Also, the timescale setting was set to 0.1 seconds. The results were produced in a similar way to the steady state simulation, with the desired contour plots and streamlines being produced. The key images which were taken were velocity contours of the model as a whole and also a chart plotting the velocity at a particular point on the model. Also, separate planes were created at various points on the model to provide a visual description of the velocity behaviour at certain points of interest along the model.

# Chapter 4

# Results

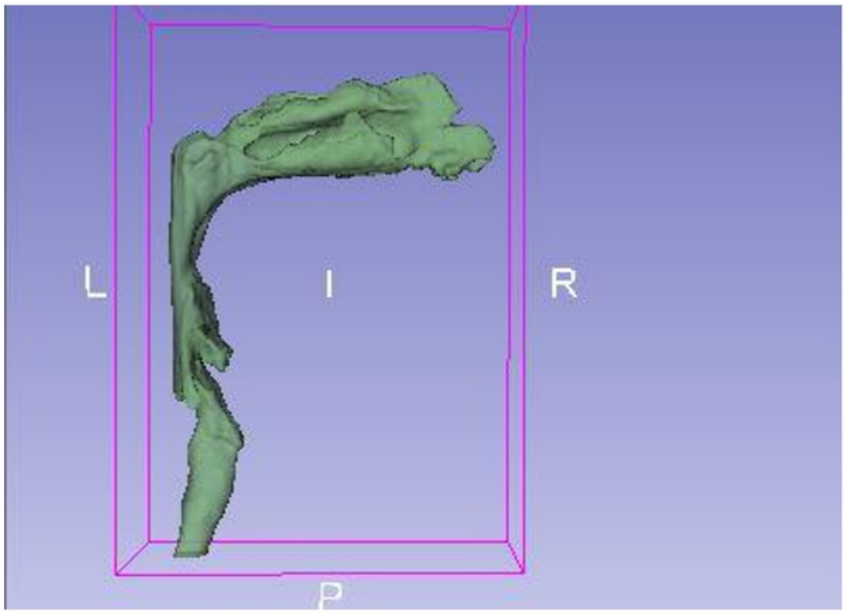


**Figure 4.1:** Nasal Model created using 3D Slicer

Table 4.1: The relevant values for the mesh convergence analysis

| MaxFaceSize | Nodes | Elements | Middle Point | Maximum Point | Mean |
|---|---|---|---|---|---|
| 0.01 | 3381 | 10675 | 1.47E+00 | 1.55E+00 | 1.42E+00 |
| 0.006 | 4441 | 13803 | 1.79E+00 | 1.79E+00 | 1.5 |
| 0.0045 | 5753 | 17761 | 1.76E+00 | 1.76E+00 | 1.45 |
| 0.004 | 6865 | 21008 | 1.78E+00 | 1.84E+00 | 1.47 |
| 0.0035 | 9200 | 27250 | 1.81E+00 | 1.86E+00 | 1.48 |
| 0.003 | 12924 | 37557 | 1.81E+00 | 1.84E+00 | 1.48 |
| 0.0026 | 16007 | 46841 | 1.83E+00 | 1.90E+00 | 1.47 |
| 0.0021 | 26625 | 75868 | 1.80E+00 | 1.86E+00 | 1.46 |
| 0.0015 | 56857 | 157122 | 1.79E+00 | 1.85E+00 | 1.46 |
| 0.0013 | 77966 | 213902 | 1.79E+00 | 1.85E+00 | 1.46 |

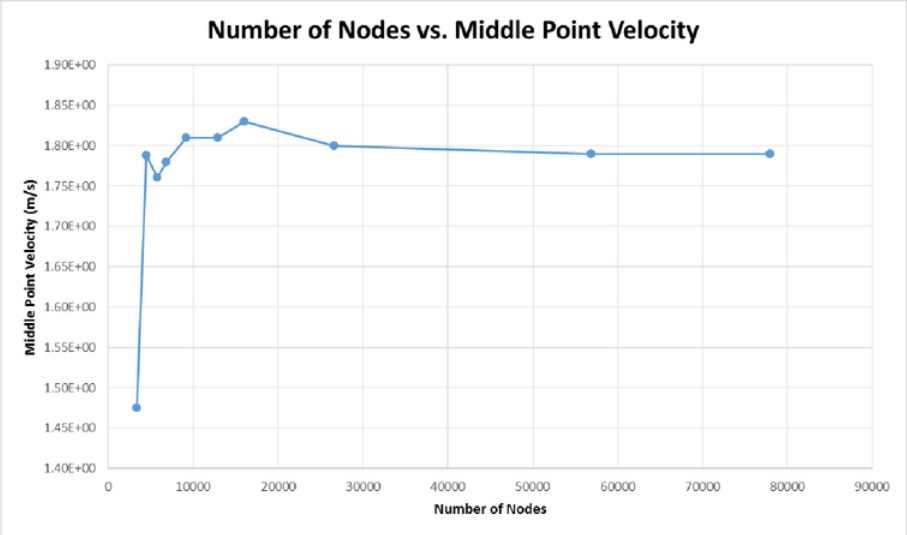


**Figure 4.2:** Middle point velocity curve to demonstrate mesh convergence

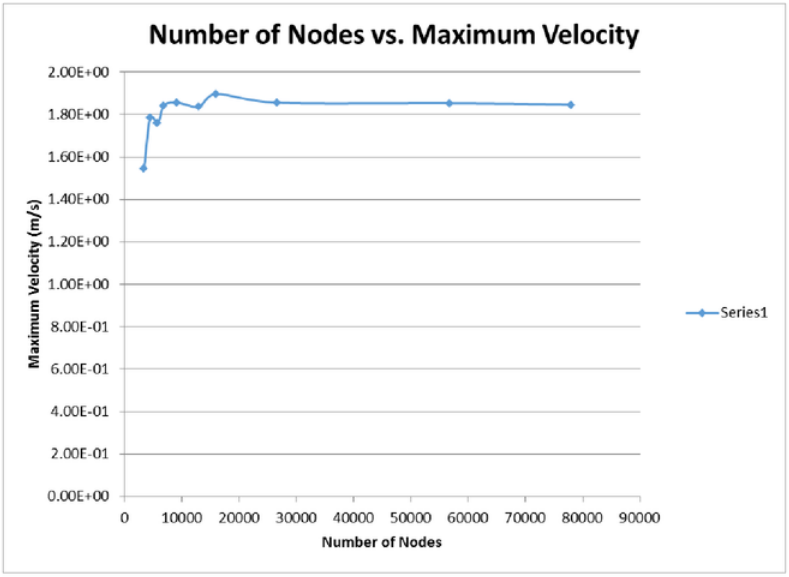


**Figure 4.3:** Maximum velocity curve to demonstrate mesh convergence

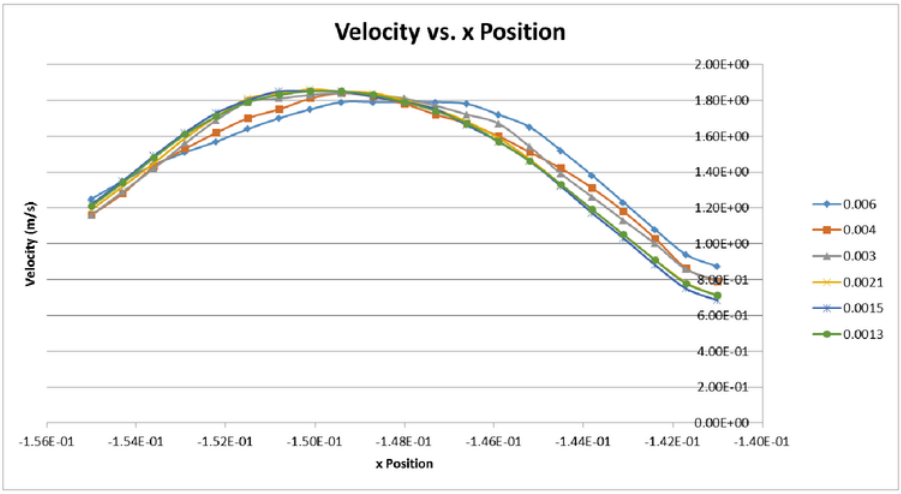


**Figure 4.4:** Velocity distribution at various mesh densities

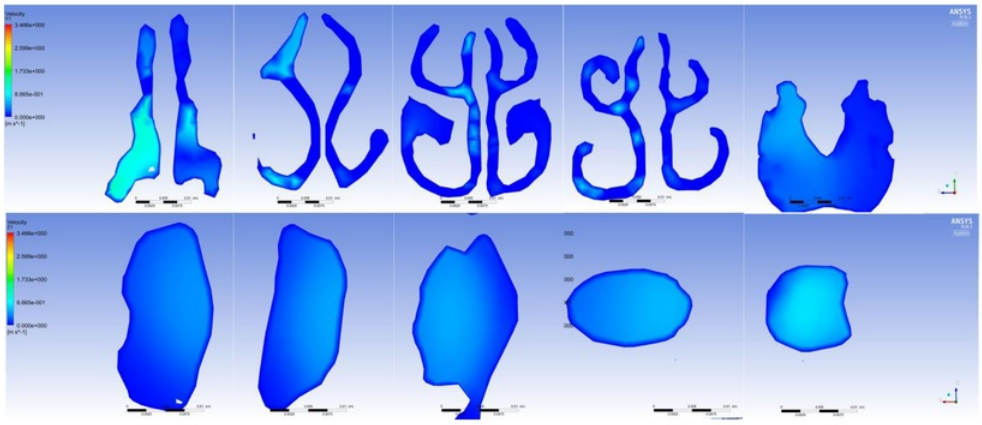

**Figure 4.5:** Coronal and Axial views of velocity simulation (elapsed time = 1 sec.)

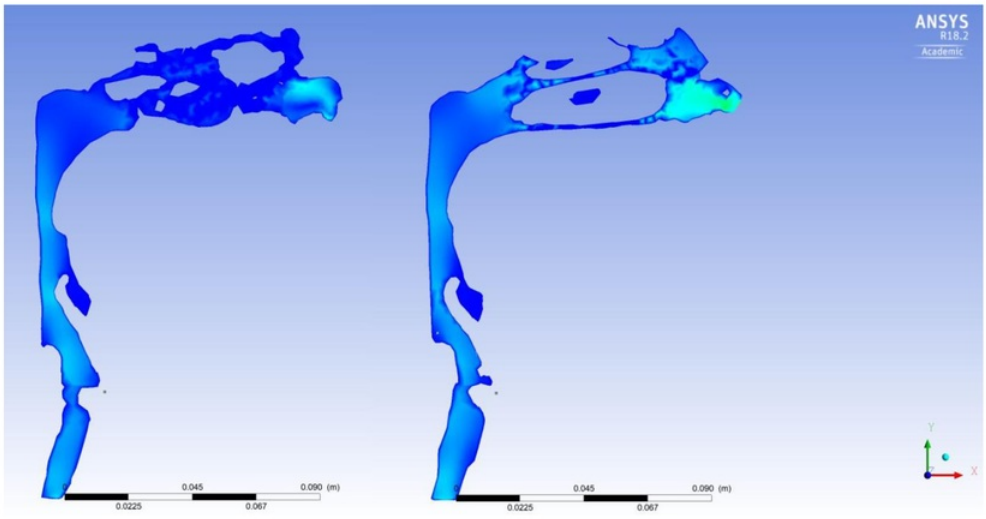


**Figure 4.6:** Sagittal view of velocity featuring left and right nasal passage (elapsed time = 1 sec.)

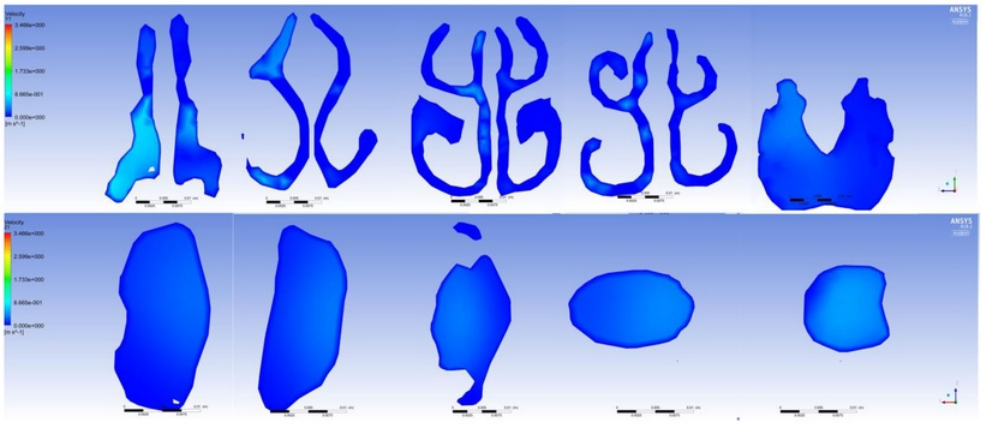

**Figure 4.7:** Coronal and Axial views of velocity simulation (elapsed time = 2 sec.)

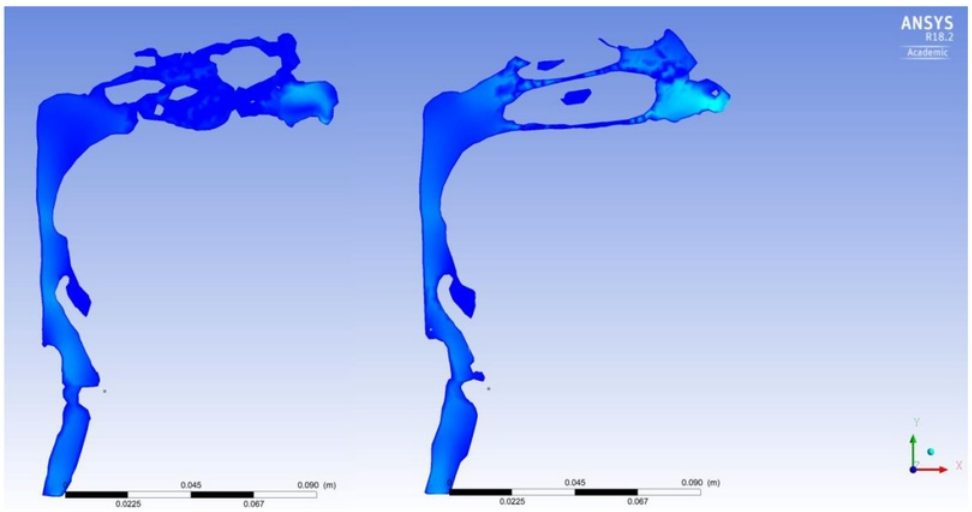


**Figure 4.8:** Sagittal view of velocity featuring left and right nasal passage (elapsed time = 2 sec.)

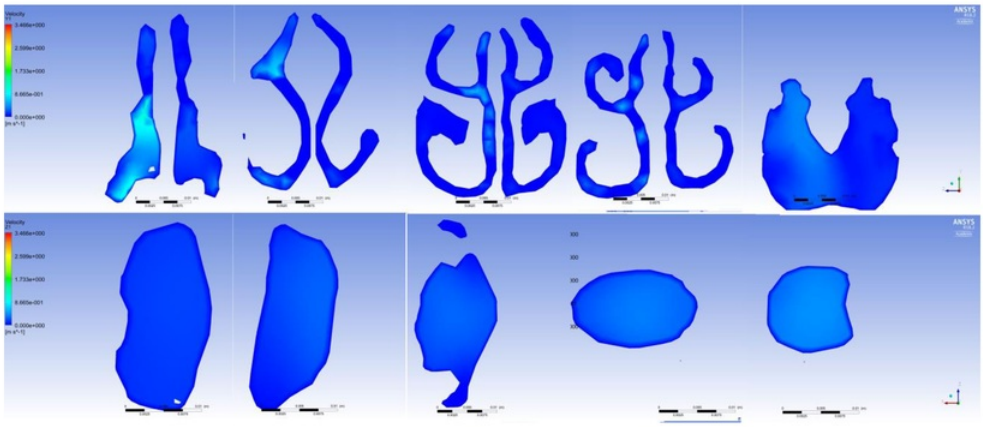

**Figure 4.9:** Coronal and Axial views of velocity simulation (elapsed time = 3 sec.)

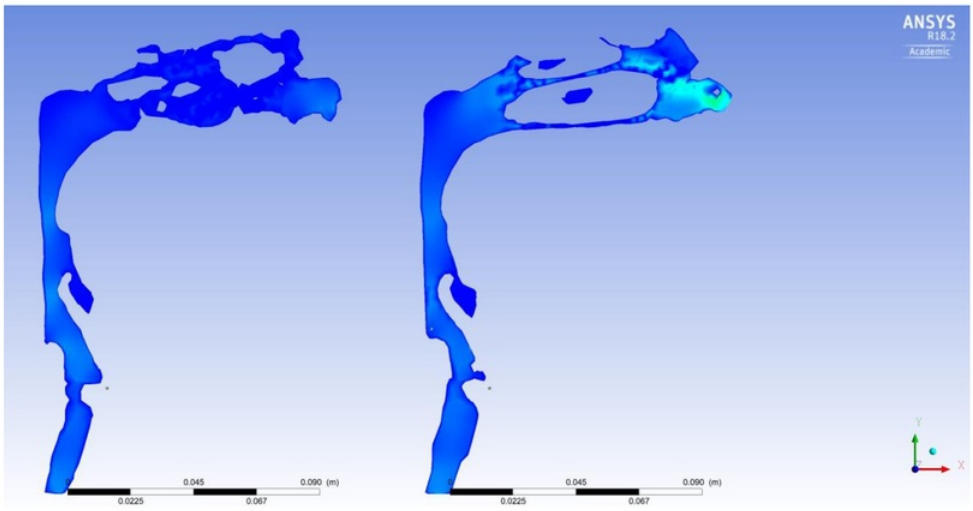


**Figure 4.10:** Sagittal view of velocity featuring left and right nasal passage (elapsed time = 3 sec.)

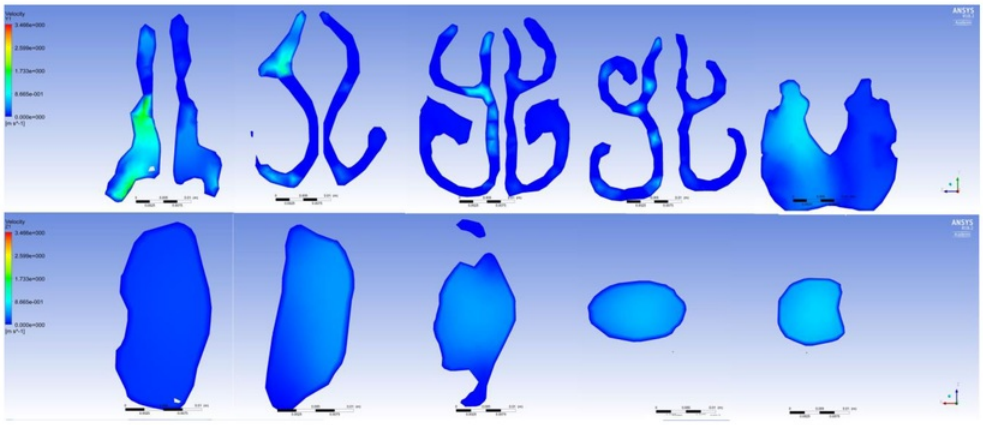

**Figure 4.11:** Coronal and Axial views of velocity simulation (elapsed time = 4 sec.)

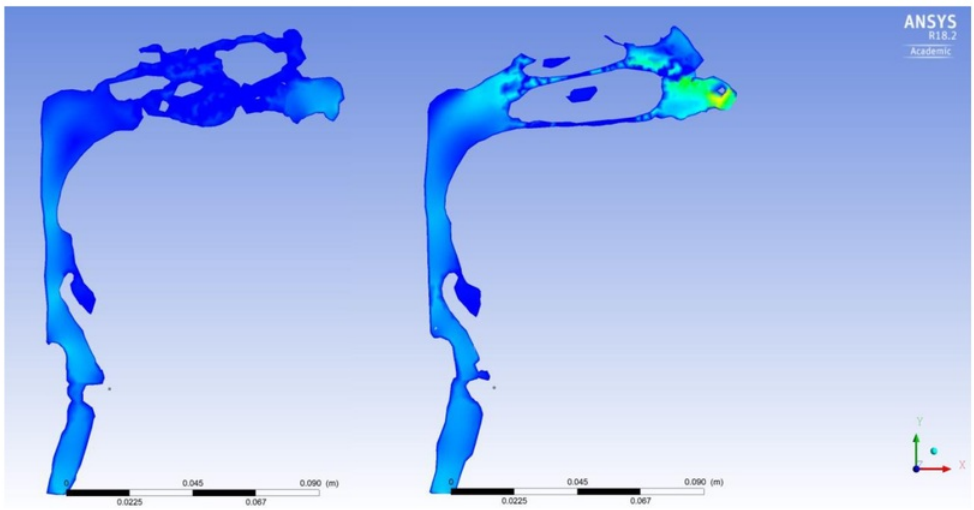


**Figure 4.12:** Sagittal view of velocity featuring left and right nasal passage (elapsed time = 4 sec.)

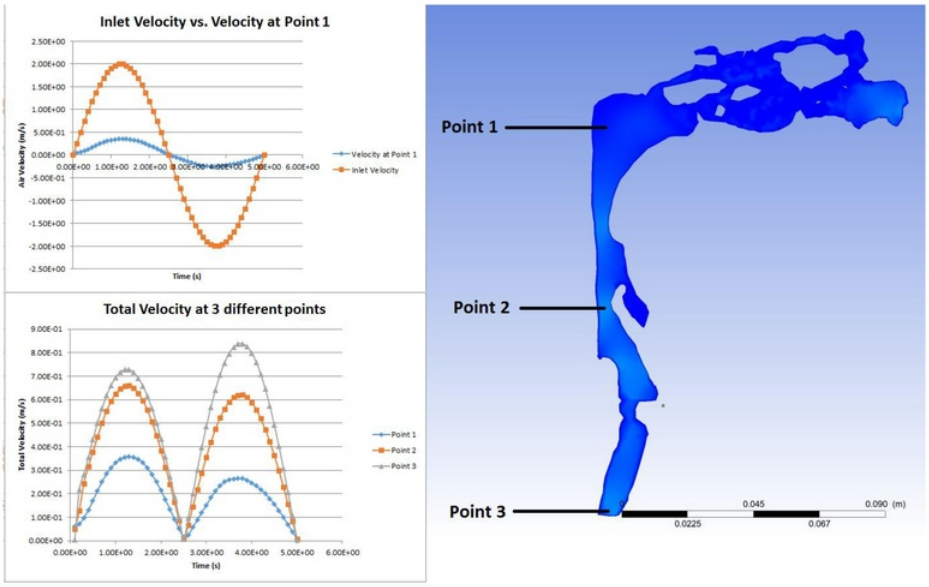


**Figure 4.13:** Graphs of Inlet Velocity vs. Velocity at Point 1 and Total Velocity at 3 points, and also the location of the three points of reference

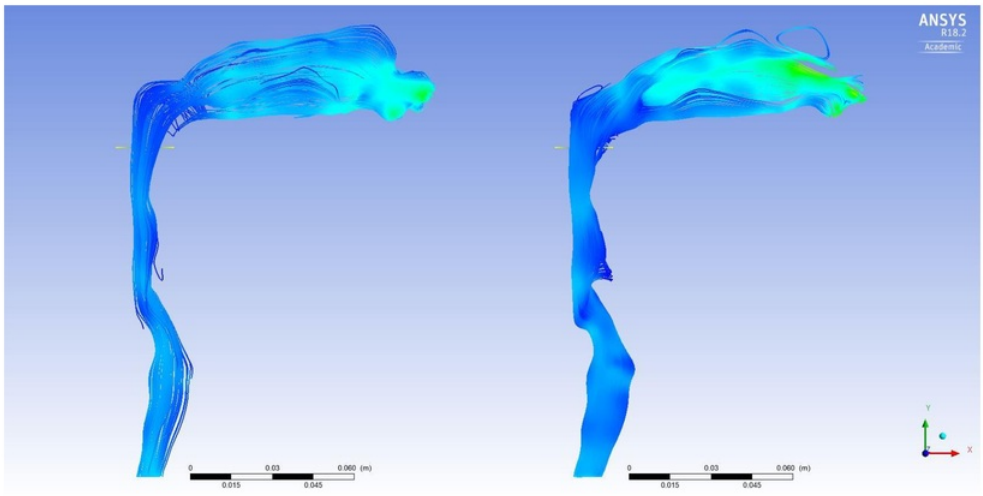


**Figure 4.14:** Velocity streamline at 1.2 and 3.7 seconds respectively

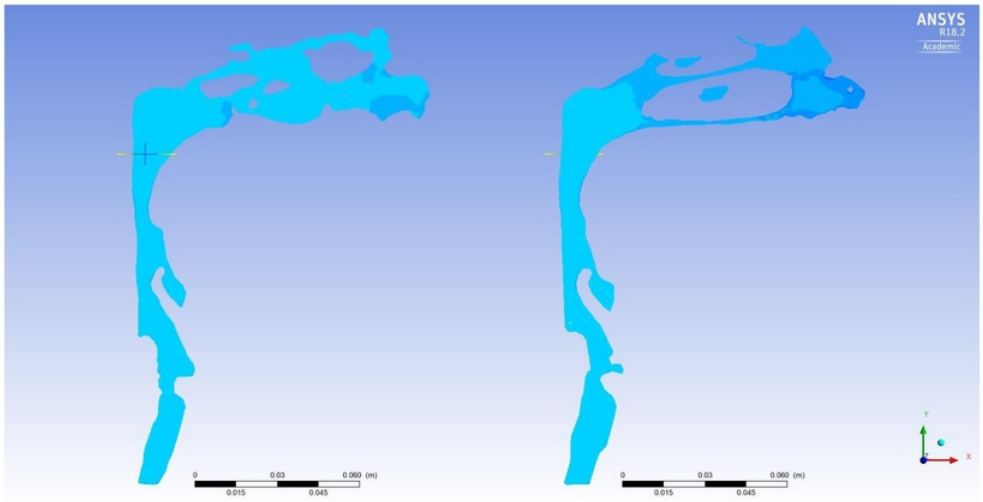


**Figure 4.15:** Total Pressure at left and right nasal passage (elapsed time = 1.2 seconds)

# Chapter 5

# Discussion

This section will discuss in detail the results presented in the previous chapter, and also provide a greater explanation of the approach taken during the method.

## 5.1 Experimental Discussion

This subsection will discuss the approach which was taken when conducting the experimental method section of the project. Techniques and approaches will be discussed along with other similar reports which were considered during this process.

When creating the model using 3D Slicer, the main aim was to not only make it accurate, but also to keep the geometry relatively simple in order to create a much more efficient CFD simulation process. One approach used to help achieve this was to use the "Fill between slices" editing effect, which meant that the time-consuming process of using the "Draw" or "Paint" effect on each slice individually could be avoided. Moreover, it also meant that the model could be much smoother than if the draw/paint method was used as this method would have a high probability of having slightly different features from slice to slice, meaning that the model would not only be rough and uneven, it would also be more complex.

Another approach which was used in order to create the model was to use other nasal models/geometry as reference. Hopkins et al. constructed a model and provided a Computed Tomography (CT) scan of one of the nasal passages as viewed from the coronal view. While creating the model, the coronal view was used in 3D Slicer to recreate the nasal cavity, and

figure 5.1 was heavily used as a guide, and the nasal geometry was traced accordingly. Similarly, Spence et al. also produced a report involving a nasal model, with an image of the final model being provided. This image was used as a guide when viewing the 3D model on the 3D Slicer screen to ensure that the model being created was as accurate as possible.

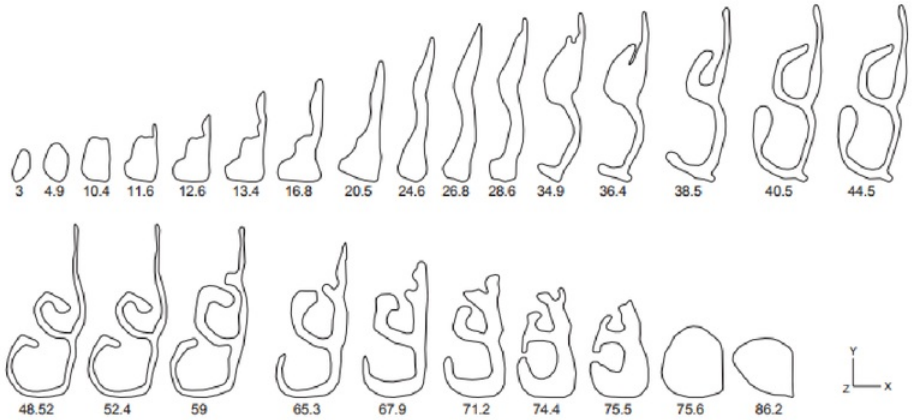


**Figure 5.1:** Coronal view of the right nasal passage at different locations [11]

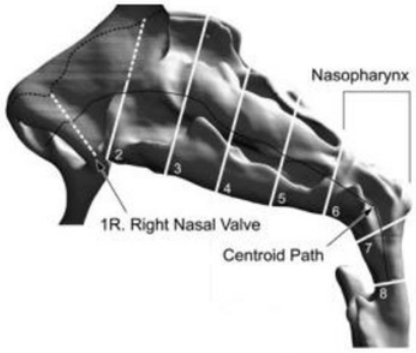


**Figure 5.2:** 3D model representation of the nasal cavity [12]

Problems began to arise when attempting to use Rhinoceros to convert the file for use in the CFD program. The file was successfully exported from 3D Slicer and could be opened in Rhinoceros as expected. However, a decision was made on the particular file type to export from Rhinoceros (IGS) which later proved to be dysfunctional when opened within ANSYS. A persistent error continued occurring relating to the reading of the model file, and was therefore determined that a new file type for the model must be used. The original file (STL) directly from 3D Slicer was also experimented with in an attempt to resolve the error ANSYS was experiencing when attempting to read the model file. This new file type did indeed solve the error of misreading the file, but a new problem arose when attempting to establish the boundary conditions of the mesh. The desired inlets and outlets were being treated as three dimensional shapes rather than a two dimensional face, meaning that the velocity simulations would not produce accurate results. Thus, the shade effect was used within Rhinoceros in order to create a more solid model which would allow the inlet and outlet conditions to be set accordingly and accurately.

## 5.2 Mesh Convergence

Before the simulations could be performed, the model had to be examined using the mesh convergence principle. A number of different mesh densities had to be applied to the model and analysed in such a way to prove that the results of the simulation are not dependent on the mesh of the model. For this process, the mesh settings were of key importance, particularly the “Max Face Size” option. This option restricted the maximum size of each element shape which together would make up a total mesh. Thus, altering this value would affect the overall density of the total mesh. The first value chosen was 0.01 as this resulted in a relatively large face size, and subsequently, a relatively low mesh density. This value therefore provided an ideal reference point to build the foundations of the mesh convergence analysis. A common velocity was applied through the nostrils of the model, and the point of measurement was taken towards the bottom of the throat as it was deemed that this area of the model was relatively stable and constant in its geometry and overall shape. This allowed

for a much more convenient and simple analysis to take place. The point of reference for the measurements was actually a straight line which passed through the model, essentially measuring the velocity across 25 points from the front wall to the back wall of the throat. These measurements at their corresponding points on the line of reference could be plotted, and produced a concave down parabolic shaped curve of results, indicating that the highest velocity occurs at the centre of the throat's cross-sectional area. The middle point and highest point of the curve are the most useful value of the curve as this would be used for the mesh convergence analysis. Since there was a slight error in the placement of the reference line, the results were skewed to the extent that the middle point of the curve was not the highest point which would ordinarily have been the case. However, a successful analysis can still take place regardless of the error.

With respect to the other max face size values, they were chosen to gradually increase the mesh density by a somewhat constant value, but as the density became much greater, the difference between values became much broader as it was becoming more evident that mesh convergence was occurring, hence the large distance between the final three points on the curve. The final max face value of 0.0013 was chosen simply for clarification that even a relatively dense mesh with a large number of elements would still produce the same results as the previously sized mesh densities which were significantly less dense.

As can be seen in figures 4.2 and 4.3, both the maximum points and middle points of each curve result in an almost reverse exponential-like shaped curve, meaning that convergence is evident as the mesh density increases. Another feature is that the three largest points of the curves feature the same value in the y direction, highlighting the accuracy of the convergence. Figure 4.4 also demonstrates mesh convergence in a similar way. The points plotted on the graph represent the velocity at each corresponding position on the x-axis of the reference line which passes through the throat area. Each curve represents the results of different mesh densities, with the key curves being that of the 0.0021, 0.0015 and 0.0013 curves. Given that the points of these curves are almost the exact same, and an almost identical curve shape to each of these three curves indicate that the results of each simulation are approximately identical, again highlighting the existence of mesh convergence.

# 5.3 Steady-State Conditions

## 5.3.1 Method Approach

The approach used was indeed a relatively basic approach with many of the basic settings within the ANSYS program being applied. After processing the results of the mesh convergence, the point of convergence based on the results was a max face size value of 0.0021 as this was the corresponding point on the curve at which convergence occurs. The significance of using this point in particular was that it was the approximately the largest possible density which could be used for the simulation without compromising the accuracy of the results. The smaller densities, as seen in the mesh convergence figures, would have produced differing results which would therefore not be entirely accurate and not useful for this project. Also, the larger densities had to be avoided in order to avoid the possibility of having the mesh become too dense which can also compromise the results. The larger density would also prove to be unnecessary as the results produced would still be very similar, but there would be a much larger simulation time as a result. Given that time management and simplification were key approaches used when undertaking this project, it was deemed that the most sensible approach would be to use the smallest possible density while still remaining within the mesh convergence region. Therefore, the corresponding max face value which was to be used for the simulation is 0.0021.

As this simulation was a simple steady-state condition, a simple singular velocity was used to act as inspiration rather than a complete breathing cycle. 3m/s as an inlet velocity was used in accordance with particular sources which performed a similar analysis (sources used values between 1 and 5 so 3 was taken as an average). The idea of a no-slip condition is that the velocity of a particular given fluid at a particular boundary will have a velocity of zero relative to the particular boundary. Therefore, for this particular simulation, the velocity of the air near the walls of the upper airway model will be equal to zero. K-epsilon is one of the most commonly used methods for conducting analysis using CFD software. It is suited to turbulent flow conditions, and given that this simulation is treated as a turbulent model and also the simplicity and widespread use of the k-epsilon method, it was deemed as the most

basic and suitable option to be used. It involves the use of two differential transport equations to conduct the analysis: one to define the turbulent kinetic energy (k), and one to define the dissipation rate of the turbulent kinetic energy (ε) [13].

### 5.3.2 Results Processing

Results were successfully produced for the steady-state simulation. The streamlines and contour plots were observed and no abnormal features were present. The contour plots did resemble the images produced in other journal articles, and the same could be said with regards to the velocity profile. However, the main purpose of creating a steady-state condition simulation was to ensure that the model and simulation worked and produced accurate results, and also to provide the foundation for the later transient flow simulation. As mentioned previously, the results from the transient flow simulation were directly linked to the steady-state simulation in order to save some time during the simulation process.

One major reason why the results from the steady-state simulation were not analysed thoroughly was due to the lack of real-world relevance of such a simulation. Many of the journal papers which have conducted similar experiments and simulations used a constant velocity or flow rate to represent simply the inspiration phase of the breathing cycle. However, the breathing cycle does in fact follow a typical sine curve, as will be explained later, and therefore a constant velocity is not an entirely accurate representation of the typical air flow through the upper airway system. This project aims to be not only a much more real-world analysis, but also will investigate the expiration phase which appears to be overlooked quite often in much of the similar journal articles given their emphasis on purely the inspiration phase of the breathing cycle. Therefore, results from the steady-state simulations of this project will not be presented to provide a greater emphasis on the transient flow results which appear to be a much more real-world simulation of the whole breathing cycle, and are therefore deemed to be much more relevant than the steady-state results.

# 5.4 Transient Flow Conditions

## 5.4.1 Method Approach

A similar approach to the steady-state conditions was used for the transient flow conditions. The analysis itself was linked to the steady-state conditions so that the setup conditions from the steady-state analysis would continue over to the transient flow analysis. This process would reduce the time needed to create a new simulation project and also the time which the program itself needs to load the data and setup the project. Time would also be reduced in the production of the results as the transient flow results would be based off the results from the steady-state analysis, meaning that one less cycle would need to be analysed as it would already have been done as part of the steady-state flow analysis.

The major difference between the two analyses in terms of the meshing conditions was the inclusion of inflation for the transient flow analysis. Inflation allows for an increase of the density only towards the boundaries of the model, meaning that the detailed and finite areas feature a much more dense mesh, whereas the wider areas of the model feature a relatively lower mesh density. This method will place a higher emphasis on the more detailed areas of the model while placing a smaller emphasis on the broader areas of the model which are not particularly complex in geometry such as the throat component of the model.

The other major difference between the two analyses is the sine function being used to represent the velocity rather than a singular value. The function used is the following;

$$V = 2\sin(2\pi t/5) \quad (1)$$

Here, the velocity (V) is defined with respect to a given time (t). The sine curve is a mathematical representation of a typical breathing cycle of a human being at rest [14]; the first parabolic curve to represent inspiration with another parabolic curve in the opposite direction to represent expiration, with a small gap of approximately 0.1 seconds in between the two curves. However, for the purpose of this simulation, the small gap was deemed as negligible in order to simplify the simulation process. Therefore, a continuous sine curve was used to represent the respiration cycle. Given that this expression therefore represents

inspiration and expiration, the inlets and outlets of the model could no longer be considered as such, and therefore had to be changed into an "opening" to act as both an inlet and outlet which is indeed the case in a typical human being's upper airway system. The timescale factor was also included in the setup of the simulation 0.1 seconds, meaning that the contour images of the model could be viewed at intervals of 0.1 seconds. This did reduce the simulation time of the model, but the main purpose was to simplify the process of viewing the separate contour images and also the animation feature within the software program. This feature provided for an animated illustration of the velocity within the nasal model as it was subject to a typical breathing cycle.

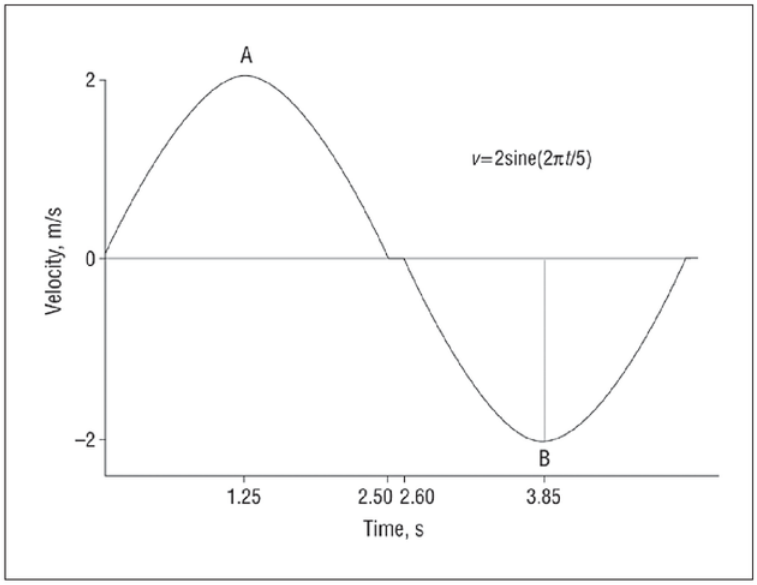


**Figure 5.3:** The sine curve used to represent the breathing cycle [14]

### 5.4.2 Results Processing

The contour results were set up in such a way to display the velocity at various points across the upper airway system at various points in time of the breathing cycle. To achieve this, five points were chosen along the nasal section of the system using the coronal view to display the images. Similarly, five points on the pharynx and larynx area were also chosen, this time displayed using the axial view. Finally, two points were chosen on the sagittal view to display a larger, two-dimensional representation of the flow through the upper airway. This view also gave an illustration of flow through each nostril in particular.

The first set of images (Figures 4.5 & 4.6) was taken at an elapsed time of one second. Zero could not be used as there would not be any air flowing through the airway as the cycle has not yet commenced, so one second was chosen instead as the first point of reference. Immediately, trends can be observed through the images being displayed. High points of the air flow velocity appear to be occurring towards the front of the nasal cavity, possibly due to the fact that the respiration cycle is still young and most of the air would be still passing through the front region of the nasal cavity, especially when considering the relatively high resistance which the air is subject to within this nasal region [4][5]. Also evident from the contour images is the difference in velocity in different regions of the airway. For example, the lower part of the upper airway appears to have a larger velocity than that of the upper section, which was also found in a similar project conducted by Tan *et al.* [15]. The sagittal images and first two coronal views do highlight a larger velocity towards the lower region of the nasal component. From the results, there also appears to be a difference in velocity between the left and right nostril. Smith conducted a similar analysis to this project and discovered that there was a difference in pressure between the two nostrils [9]. Given that there is a difference in velocity between the two nostrils, there would be enough to suggest that there would also be a difference in pressure between the two nostrils, meaning that there is a similarity between the results so far presented in this project to other projects.

At the elapsed time of two seconds (Figures 4.7 & 4.8), similar results could be found as with the results from one second. Much of what was discussed above could also be observed here, however the overall velocity was noticeably less than after one second had elapsed. Given

that on the curve, the highest velocity occurs at 1.25 seconds, the elapsed time of one second is much closer to the elapsed time of two seconds, and therefore, it should be expected that the larger velocity occurs at one second rather than two. Also given that an elapsed time of two seconds is still within the inspiration phase of the breathing cycle, it should be expected that the overall results as a whole are not too dissimilar to the results produced after one second.

Similar results can be seen after an elapsed time of three seconds (Figures 4.9 & 4.10). Despite the change in direction of the velocity, there appears to be very little difference in the contour images between the elapsed times of two and three seconds. The high velocity points seem to appear at the same points of the airway model, indicating that there has been little to no effect caused by the change in direction of the velocity. However, it was expected that the magnitude of the velocities should be approximately equal. Given that both elapsed times are the same distance from their respective peaks on the sine curve, it should be no surprise that the magnitudes of the respective velocities are indeed approximately equal.

The images produced at an elapsed time of four seconds (Figures 4.11 & 4.12) give a much greater indication of the behaviour of the velocity throughout the upper airway system. Again, the trends discussed in the previous images can also be observed here after an elapsed time of four seconds, but there are some trends which are much more exaggerated than in previous contour images. Again, results from the project conducted by Tan *et al.* showed that the velopharyngeal area was the site of the maximum velocity [15]. Although it is not clear as to whether it is indeed the highest velocity, the sagittal images show that the velopharyngeal area does indeed feature a generally higher velocity when compared to other areas of particularly the pharynx and larynx region. As mentioned in the background section, the velopharynx is the region of the upper airway where the oral and nasal cavities meet, so since this model neglects the oral cavity in the breathing cycle, the results would be likely to change if the oral cavity was used during the simulation. Other similar experiments have also proven that when considering the pharynx and larynx components of the upper airway system, the highest velocity occurs in regions where the cross-sectional area is minimal [13][15]. Results from the project of Tan *et al.* concluded that the narrower sections of the pharyngeal airway did indeed result in a larger total airflow velocity in the upper airway

system [15]. Similarly, an experiment conducted by Mihaesu *et al.* also concluded that the location of the smallest cross-sectional area did indeed result in the highest axial velocity [13]. The contour images, particularly evident in those after four elapsed seconds, highlight these ideas found in similar projects that a higher velocity is present in areas where there is a decrease in the cross-sectional area, particularly within the pharynx region. Figure 4.13 also highlights this by comparing the velocity at different points. Point 1 – located towards the top of the pharynx – features a much wider cross-sectional area than points two and three, and correspondingly features a much smaller velocity in comparison. Point 2 in particular is located around the epiglottis region highlighting the high velocity present in this area. Another similar experiment conducted by Huang *et al.* showed there was also a significant increase in velocity around the glottis area [16]. This is also evident in the contour images presented in this report, indicating that an increase in velocity is not only as a result of change in cross-sectional area, but also a change in direction of the upper airway system. Areas such as the glottis do feature some relatively sharp curves in comparison to other components particularly of the pharynx and larynx, and also feature a relatively higher velocity in these regions. This can also be observed in figure 4.14 which displays the velocity streamline. Again, there are various changes in velocity, particularly in areas which are smaller in cross-sectional area. However, it also appears that a higher velocity also occurs in areas where the airway turns relatively sharply to induce a change in velocity.

Another feature was the highest velocity appears to occur towards the front of the nasal cavity. This is clearly visible when observing the images after an elapsed time of four seconds. The theory suggests that the largest velocity occurs within the nasal valve region which is located towards the entrance of the nasal cavity. Therefore, the contour plots presented here do validate and adhere to the background theory. Figure 4.13 also validates this theory. The sine curve which was used as the inlet velocity is compared to point 1 which is located at the top of pharynx – after the air has passed through the nasal cavity. The two curves highlight the difference in velocity and the large difference between them, validating that the highest velocity would occur near the inlet, confirming the reason as to why the highest velocity occurs in the nasal valve region.

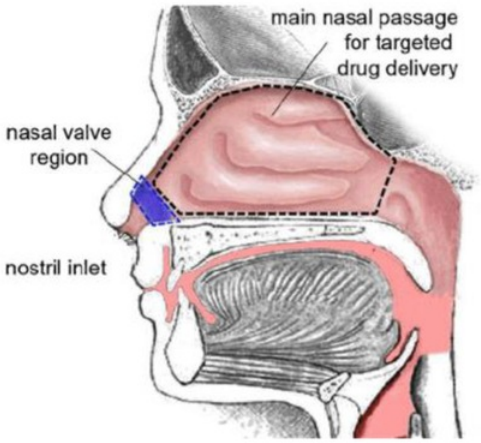


**Figure 5.4:** Location of the nasal valve region [17]

Another feature to discuss is that of pressure. As mentioned above, one of the journal articles discovered that there was a difference in pressure between the left and right nasal passage. It was evident that there was a difference in the velocities, and figure 4.15 also shows that there is indeed a difference in pressure between the two nasal passages. There is also a difference in pressure when comparing the nasal cavity and the pharynx which is expected when considering the difference in velocity between the two. This would indeed result in a different amount of pressure. However, there is an issue with investigating the pressure in this simulation. The walls of the airway structure are static and do not contract and expand like the structure would do in reality. The expanding, contracting and other movements which the structure completes would influence the pressure within the upper airway system, and although these movements are indeed relatively minor at a normal breathing rate, it would be enough to alter the results somewhat, meaning that the results from this simulation would not be entirely accurate, and are therefore not investigated further in this report.

One feature which is important to note is the lack of or minimal velocity which passes through the meatuses within the nasal cavity. This was evident when observing all of the contour images from each of the different points of elapsed time. Projects conducted by Smith and Kelly *et al.* also made the same observation [9][18]. Kelly concluded that the

process of delivering air to the lungs is a quick and direct process, and the majority of the air would therefore travel via the main passageways in the nasal cavity rather than much narrower passages such as the meatuses [18]. Kelly then went on to conclude that the meatuses would likely function in order to serve other purposes such as thermal, humidification, or even to assist with the sense of smell, rather than act as an airway passageway [18].

Given the various features explained above, there are a number of trends which occur within the upper airway system i.e. general velocity high spots and low spots. However, given the effect that certain components have on the velocity, there is enough to suggest that differences in geometry from person to person would indeed have an effect on the velocity and overall flow of air. Parameters such as diameters, lengths, angles and other geometric quantities which can be measured within the upper airway do indeed vary from person to person and would also affect the velocity flowing through the upper airway system.

There were however some observations made which were not expected. For example, towards the front of the nasal cavity, it did appear to follow the trend of having a higher velocity in the lower part of the nasal cavity than the upper part. However, towards the back of the nasal cavity, the opposite appeared to be the case, with a larger velocity towards the upper part of the nasal cavity, rather than the lower part. Given that this is representing the expiration phase of the breathing cycle, the air is therefore travelling upwards from the pharynx into the nasal cavity. The air travelling into the lower part of the nasal cavity therefore has a much sharper curve to follow than the air travelling into the upper part. The reason for the difference in velocity could be due to the air entering the lower part of the nasal cavity having to travel slower than the air entering the upper part in order to be able to navigate the sharper change in direction.

Some of the unexpected results could be put down to the choice of mesh. Although the mesh convergence did prove that the accuracy of the results was still constant regardless of the mesh density, a much finer mesh however may have provided a more detailed illustration of the airflow through the model. Some of the similar projects did mention in their respective journal articles that a fine or high mesh density was used for the presentation of the results.

As mentioned previously, there was an approach taken during the completion of this project to keep the process as simple as possible, meaning that some of the settings within the analysis program could possibly have produced different results if used in the correct way.

Some unexpected results could also be put down to the choice of method used for the simulation. There were varying conclusions as to whether the k-epsilon method was suited to a simulation such as this one. For example, projects such as those conducted by Mihaesu *et al.* and Aasgrav *et al.* utilised the k-epsilon method and successfully reached their desired conclusions [13][19]. However, there were projects conducted, such as those conducted by Rahiminejad *et al.* and also Mylavarapu *et al.* determined that in fact the k-ω method was better suited to a simulation such as this [20] [21]. Given the evident mixed opinions on the k-epsilon method, it is a possibility that this method is the cause of the some of the abnormal results being presented.

## 5.5 Limitations

Naturally, as with all projects, there were indeed some limitations which would have some effect on the outcome of the project, and this project is no different. The first limitation would be the approach taken when creating the model itself using 3D Slicer. As mentioned in previous sections of this report, the approach taken was to simplify the geometry of the model. While using this approach did eventually result in a satisfactory model being produced, the simplifying of the model could have potentially compromised the accuracy of the model. Because of the simplified method, the DICOM images of the specific upper airway were not traced exactly and therefore the model itself is not an exact replica of the specific upper airway provided by the images. However, the DICOM images being used also had to remain confidential while conducting the project, and therefore, directly copying the upper airway from these images could potentially jeopardise the confidentiality of this project. Therefore, there were some limitations present during the creation of the model phase of the project.

Some limitations were also potentially present during the simulation phase of the project. As mentioned previously, only basic and default settings were applied to the simulation. Many other settings within the software program were not used or explored and thus could potentially have restricted the accuracy of the results somewhat. This was due to the simplistic approach taken when conducting the simulations and thus could be considered as a potential limitation for the project.

Another possible limitation was determining the exact point of the mesh convergence. Given that only a certain number of points were trialled when conducting the mesh convergence experiment, it is unlikely that the exact point of mesh convergence was found. If the exact value where the mesh converges was found, it could be used for the later simulations, not only providing slightly different results, but also a shorter simulation time given that the mesh density will be smaller than that used for the simulations in this project.

One quite significant limitation present during the simulation phase of the project was the relatively extensive time taken by the software program to setup and run the simulation. There was much time spent waiting for the program to work these functions, and thus, some of the limitations listed above were caused as a result of the extensive time taken by the program to setup and run the simulations. For example, if the setup and running time were much shorter, the time saved could have been spent on trialling various other settings within the simulation setup in an attempt to possibly increase the accuracy of the results. Given that the allocated time for the completion of this project was relatively short, it was deemed unfeasible to experiment with all the various settings due to the long waiting time for the setup and simulation to take place. Similarly, more time could also have been spent on the mesh convergence phase of the project in order to trial more mesh density sizes to get closer to the exact point of mesh convergence. Both these limitations involve simple trial and error, but were deemed unfeasible for this project due to the lengthy time taken by the CFD program to setup and run the simulation to produce the desired results.

Another possible limitation is the treatment of the model by the simulation program. The program assumes that the wall of the model is a “hard” wall, but in reality, it is surrounded by tissues and other soft bodily materials [22]. As mentioned in the background section, the surrounding walls of the upper airway system tend to collapse and manipulate its own shape

in order to assist with the breathing process, but this cannot be replicated in the simulation software. Although the changes to the structure under normal breathing conditions would only be minor, this particular behaviour of the upper airway system cannot be observed, nor can the interaction between the system and the passing air.

# Chapter 6

# Conclusions

The upper airway system and analysis of such a structure has often been overlooked in terms of its importance to relevant issues such as the transportation of medical drug particles. Analysis of this structure would therefore help develop a greater understanding of the structure, and therefore open the door for such issues to one day be properly addressed.

A model was successfully created and simulations were run to replicate a typical breathing cycle. Most of the results produced from the simulation did match the theoretical concepts discussed in this report and were also comparable with other similar projects which were previously conducted. These results alone were enough to prove that the simulation can successfully be achieved and produce reliable results. There were found to be trends which generally occur within the upper airway but also indications that the specific geometry of the airway which varies from person to person would have an effect on the overall velocity passing through the airway. Work in the future could therefore be done in order to achieve greater personalisation for each person's specific needs.

The production of some unusual results indicates that this topic can indeed be investigated much further in order to achieve an even greater understanding. This project therefore can be used as a foundation to not only build a basic understanding, but also for further research to subsequently be conducted into a variety of different areas.

## 6.1 Further Work

In terms of work which could be conducted to further investigate the concepts and results produced from this project, the main method to achieve this is to address the issues which were raised in the previous section of this report when discussing the limitations of this project. The level of detail is one area which could be improved for example. As mentioned previously, the approach taken was to keep both the creation of the model and the simulation as simple as possible without significantly compromising the accuracy and reliability of the results. Although it was deemed that the results presented here were indeed valid and reliable, there is indeed room for improvement in terms of the detail which the project was conducted which could have an effect on particularly the accuracy of the results. Similarly, the simulation process was also simplified with only basic settings being used for the simulation process in order to achieve an ideal time effectiveness of project completion. Therefore, one major way to improve upon this particular project would be an increase in time allocation to complete the project. A larger time allocation would allow for more time to investigate the various features offered within the CFD program in order to observe the difference provided by the various features available. There would also therefore be a justification for the investigation of these different features when considering the long elapsed time taken by the program to complete the simulation. During the completion of this project, it was deemed unfeasible to run multiple simulations using various different settings as it was deemed that too much project time would be lost by having to wait for the program to complete the simulations. Therefore, a longer time allocation to complete the project would provide possibly more accurate results, and more time to experiment with the various different features offered within the CFD program.

Another method to consider for possible future work would be to create multiple nasal models and to conduct direct comparisons between them. One potential issue with this project is that the model and results presented here are compared with the work of others. There is potentially a lack of consistency as there are some differences between the projects which could influence the results somewhat. For example, different people are conducting the experiment and would therefore have a different approach to their project compared to this

one. Also, different programs were used to create the model meaning that there could be some differences between the models based on the program they were created using. Similarly, given the age of some of the reports used as reference, there could also be a difference in the quality of the CFD programs being used. Although some used the same software program, the difference in age between some is quite significant, and therefore, a much newer version featuring the latest updates could also provide a difference in results. Therefore, if multiple models were made by the same user, direct comparisons can be drawn with a smaller possibility of inconsistency.

# Appendix A

# Consultation Meetings Attendance Form

**Consultation Meetings Attendance Form**

| Week | Date | Comments (if applicable) | Student's Signature | Supervisor's Signature |
|---|---|---|---|---|
| 1 | 2/8/17 | Met to kick off the project | Matthew Berg | |
| 2 | 7/8/17 | Worked on the model | Matthew Berg | |
| 3 | 14/8/17 | Met with Joel to progress | Matthew Berg | |
| 4 | 21/8/17 | Met with Joel to make some improvements | Matthew Berg | |
| 5 | 28/8/17 | Met with Joel to finish model | Matthew Berg | |
| 6 | 5/9/17 | Met with James to start converting the file | Matthew Berg | |
| 7 | 14/9/17 | Showed Shaohoon the model | Matthew Berg | |
| Mid-sem | 19/9/17 | Discussed meshing options with Shaohoon | Matthew Berg | |
| 8 | 6/10/17 | Met with James to work on CFD | Matthew Berg | |
| 9 | 12/10/17 | Discussed progress and future work | Matthew Berg | |
| 10 | 17/10/17 | Worked with James on CFD | Matthew Berg | |
| 11 | 23/10/17 | Worked on CFD | Matthew Berg | |
| 12 | 1/11/17 | Discussed with Shaohoon how to finish project | Matthew Berg | |

# References

[1] K. Nikander, D. Von Hollen, H. Larhrib. “The size and behavior of the human upper airway during inhalation of aerosols”, Expert Opinion on Drug Delivery, vol. 14, no. 5, pp. 621-630, 2017.

[2] P. Karakosta, A. Alexopoulos, C. Kiparissides. “Computational model of particle deposition in the nasal cavity under steady and dynamic flow”, Computer Methods in Biomechanics and Biomedical Engineering, p.1-13, 2013.

[3] C. Squier, M. Kremer. “Biology of Oral Mucosa and Esophagus”, JNCI Monographs, vol. 21, pp. 7-15, 2001.

[4] R. Pearce, C. Worsnop. “UPPER AIRWAY FUNCTION AND DYSFUNCTION IN RESPIRATION”, Clinical and Experimental Pharmacology and Physiology, vol. 26, no. 1, pp. 1-10, 1999.

[5] A. Sahin-Yilmaz, R. Naclerio. “Anatomy and Physiology of the Upper Airway”, Proceedings of the American Thoracic Society, vol. 8, no. 1, pp. 31-9, 2011.

[6] J. Rau, “The Inhalation of Drugs: Advantages and Problems”, Respiratory care, vol. 50, no. 3, pp. 367-82, 2005.

[7] R. Dal Negro, “Dry powder inhalers and the right things to remember: a concept review”, Multidisciplinary respiratory medicine, vol. 10, no. 1, pp.13, 2015.

[8] M. Ibrahim, R. Verma, L. Garcia-Contreras. “Inhalation drug delivery devices: technology update”, Medical Devices: Evidence and Research, vol. 8, p.131(9), 2015.

[9] K. Smith, “CFD Analysis of Pressure and Flow Characteristics of the Human Nose”, M.S. thesis, Worcester Polytechnic Institute, Worcester, MA, 2008.

[10] D. Lewis, "REVIEWING CURRENT THINKING ON THE IN VIVO BEHAVIOUR OF PARTICLES IN THE EXTRA-FINE REGION", Chiesi Ltd, Manchester, United Kingdom, 2015, pp. 4-9.

[11] L. Hopkins, J. Kelly, A. Wexler, A. Prasad, "Particle image velocimetry measurements in complex geometries", Experiments in Fluids, vol. 29, no. 1, pp.91-95, 2000.

[12] C. Spence, N. Buchmann, M. Jermy, S. Moore, "Stereoscopic PIV measurements of flow in the nasal cavity with high flow therapy", Experiments in Fluids, vol. 50, no. 4, pp.1005-1017, 2011.

[13] M. Mihaescu, S. Murugappan, E. Gutmark, L. Donnelly, S. Khosla, M. Kalra, "Computational Fluid Dynamics Analysis of Upper Airway Reconstructed from Magnetic Resonance Imaging Data", Annals of Otology, Rhinology & Laryngology, vol. 117, no. 4, pp.303-309, 2008.

[14] S. Ishikawa, T. Nakayama, M. Watanabe, T. Matsuzawa, "Visualization of Flow Resistance in Physiological Nasal Respiration: Analysis of Velocity and Vorticities Using Numerical Simulation", Archives of Otolaryngology–Head & Neck Surgery, vol. 132, no. 11, pp.1203-1209, 2006.

[15] J. Tan, J. Huang, J. Yang, D. Wang, J. Liu, J. Liu, S. Lin, C. Li, H. Lai, H. Zhu, X. Hu, D. Chen, L. Zheng, "Numerical simulation for the upper airway flow characteristics of Chinese patients with OSAHS using CFD models", European Archives of Oto-Rhino-Laryngology, vol. 270, no. 3, pp.1035-1043, 2013.

[16] J. Huang, H. Sun, C. Liu, L. Zhang, "Moving boundary simulation of airflow and micro-particle deposition in the human extra-thoracic airway under steady inspiration. Part I: Airflow", European Journal of Mechanics / B Fluids, vol. 37, pp.29-41, 2013.

[17] K. Inthavong, M. Fung, X. Tong, W. Yang, J. Tu, "High Resolution Visualization and Analysis of Nasal Spray Drug Delivery", Pharmaceutical Research, vol. 31, no. 8, pp.1930-1937, 2014.

[18] J. Kelly, A. Prasad, A. Wexler, "Detailed flow patterns in the nasal cavity", Journal of applied physiology, vol. 89, no. 1, pp.323-37, 2000.

[19] E. Aasgrav, S. Johnsen, A. Simonsen, B. Müller, "CFD simulations of turbulent flow in the human upper airways", presented at 12th Int. Conf. on CFD in Oil & Gas, 2017, Trondheim, Norway. 2017

[20] M. Rahiminejad, A. Haghighi, A. Dastan, O. Abouali, M. Farid, G. Ahmadi, "Computer simulations of pressure and velocity fields in a human upper airway during sneezing", Computers in Biology and Medicine, vol. 71, pp.115-127, 2016.

[21] G. Mylavarapu, S. Murugappan, M. Mihaescu, M. Kaira, S. Khosla, E. Gutmark, "Validation of computational fluid dynamics methodology used for human upper airway flow simulations", Journal of Biomechanics, vol. 42, no. 10, pp.1553-1559, 2009.